REVIEW

A review on chemical precipitation in carbon capture, utilization and storage

Jui-Yen Lin[1], Erica A. Garcia[2], Florencio C. Ballesteros Jr.[2], Sergi Garcia-Segura[3] and Ming-Chun Lu[4*]

Abstract

Carbon capture, utilization, and storage (CCUS) technologies are being developed to address the increasing CO_2 emissions, mitigating the global warming and climate change. In this context, chemical precipitation has been advanced to enhance the performance, energy-efficiency and profitability of CCUS. In this review, we first present the fundamentals of precipitation and dissolution, and then summarize the incorporation of precipitation in each aspect of CCUS. The controlled precipitation of CO_2-rich solid during the capture of CO_2 by regenerable solvents can reduce the energy demand. The mineral carbonation of silicate and industrial waste sequestrates CO_2 as stable solids. The efficiency of mineral carbonation, either direct or indirect, is dictated by the dissolution of minerals and the precipitation of carbonates and silica. The precipitation of calcium carbonate can be controlled to produce various polymorphs and morphology, enabling its utilization for the enhancement of profitability and environmental benefits. Ultimately, the prospective for future research was proposed.

Keywords: CO_2 absorption, Mineral carbonation, Calcium carbonate, Dissolution, Chemical precipitation

1 Introduction

The substantial emission of greenhouse gases from anthropogenic activities has been attributed to the global warming and climate change. The atmospheric concentration of carbon dioxide (CO_2), the major anthropogenic greenhouse gas, has increased from the preindustrial level of 280 to 420 ppm in March 2022 due to the extensive use of fossil fuels [1]. According to the data of American National Oceanic and Atmospheric Administration, the annual growth rate of CO_2 in the 2010s was averaged to be 2.4 ppm, which can be faster considering that the global energy demand is projected to increase by 50% in 2050 [2]. Recently, the Intergovernmental Panel on Climate Change (IPCC) suggested that the global warming of 1.5 °C, instead of 2 °C, is necessary to minimize the climate change to a limited level. To meet that goal, the IPCC estimated that the net anthropogenic emission of CO_2 has to decrease 45% of 2010 levels in 2030 and the net zero should be realized in 2050 [3]. Therefore, it is imperative to reduce the CO_2 emission during the energy transition period before the renewable energy replaces the fossil fuels.

Carbon capture, utilization, and storage (CCUS) have been explored extensively to provide technologies for CO_2 reduction [4, 5]. The capture of CO_2 using regenerable solvents from the exhaust gas of fossil fuel combustion, steel making, and concrete production is the first step of CCUS to produce high-purity CO_2 stream. Basic solvents such as amines have been explored to capture the CO_2 from post-combustion gas; the regeneration of the amines is accomplished at elevated temperature and pressure to produce high-purity CO_2 stream [6]. The CO_2 stream can further be utilized as feedstocks in electro- and thermo-catalytic conversion, acidifying and extracting agent in food industry, and as fracking agent for enhanced recovery of oil and shale gas [7]. Alternatively, the CO_2 can be captured and utilized by the biotic route, mainly by microalgae and the following biorefinery [8].

*Correspondence: mmclu@nchu.edu.tw

[4] Department of Environmental Engineering, National Chung Hsing University, Taichung 40227, Taiwan
Full list of author information is available at the end of the article

The conventional storage of CO_2 can be accomplished by injecting the captured CO_2 into geological sinks, which requires a suitable reservoir with appropriate porosity, permeability, and thickness, a cap rock with sufficient sealing efficiency, and high geological stability [9]. Moreover, constant monitoring is required to detect any potential leakage of CO_2 from geological sink [10].

Many advances have been explored to enhance the cost-effectiveness of CCUS, including the control of precipitation phenomenon [11, 12]. The chemical precipitation can be implemented to improve the CCUS in different ways. The regeneration of CO_2-rich solvent is one of the most energy-intensive processes in CO_2 capture. The controlled precipitation of CO_2-rich precipitate can reduce the heat duty of regeneration as the amount of solvent to be regenerated is reduced [13, 14]. The potential leakage of stored CO_2 and the cost of post-storage monitoring can be circumvented by the precipitation of carbonate minerals, known as mineral carbonation. Since the carbonized precipitate is thermodynamically stable, the long-term storage stability can be ensured without constant monitoring [15]. Moreover, the choice of feedstocks of mineral carbonation is versatile, ranging from natural minerals to mining and industrial wastes [16]. The produced precipitates can be utilized in different industries, creating additional revenues to enhance the overall cost-effectiveness and reduce the environmental impact. Despite that many reviews are present to cover each topic in detail [7, 16–18], this review aims to provide a bigger picture about the incorporation of precipitation in CCUS (Fig. 1), especially the capture of $CO_2$ by solid-forming regenerable solvents, sequestration of CO_2 by mineral carbonation, and the utilization of precipitated carbon carbonate.

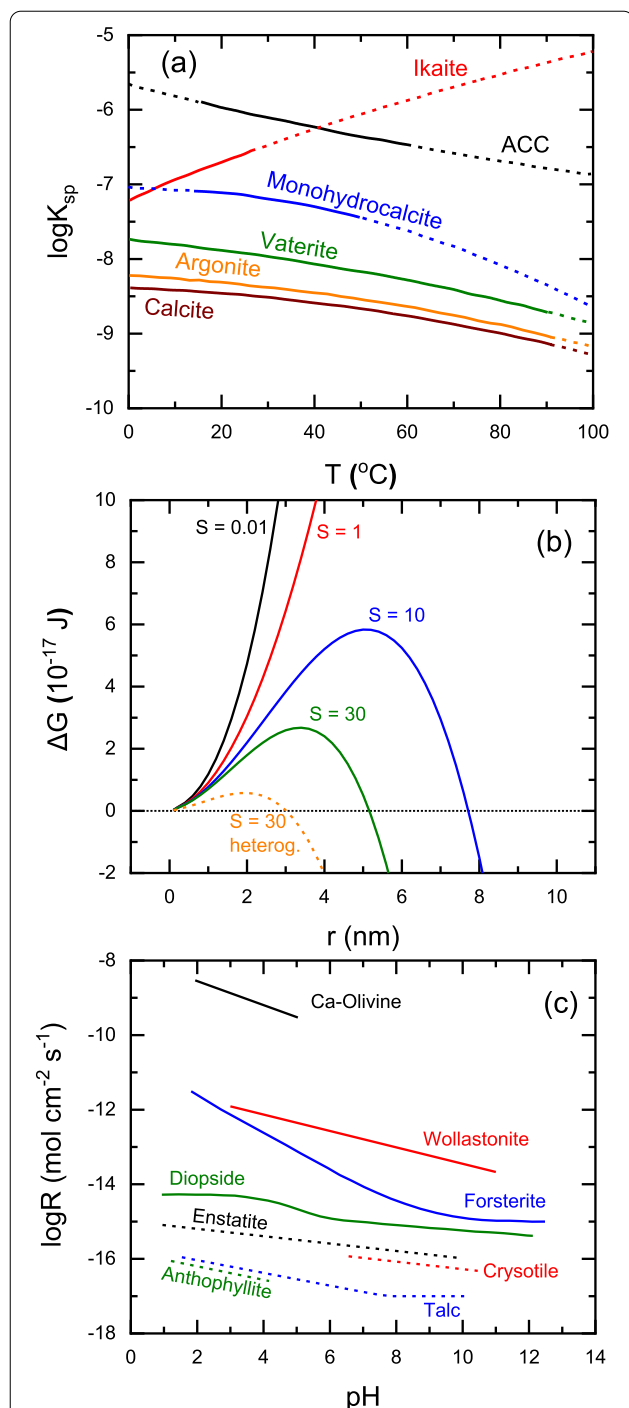## 2 Principle of precipitation and dissolution

The thermodynamic driving force of precipitation in solution is described by the change in the Gibbs free energy, the difference between the chemical potential of the dissolved solute (μ_1, J mol^{-1}) and solid (μ_2, J mol^{-1}) (Eq. 1) [19]. Under constant temperature and pressure, the difference in chemical potential is expressed by the supersaturation ratio (S). For a sparingly soluble ionic solid $A_\alpha B_\beta$, S is defined as the ratio of activity product (Q) to solubility product (K_{sp}). The precipitation route depends on the degree of supersaturation, being homogeneous nucleation in labile zone and crystal growth in metastable zone. The strategy to bring the system to supersaturation scenario includes the change in temperature, pH, and composition [20]. The temperature alters the K_{sp} according to the van't Hoff equation. In the case of calcium carbonate, nearly all of the polymorphs show smaller K_{sp} as temperature increases as depicted in Fig. 2a [21]. For protonatable species like CO_3^{2-}, the solution pH dictates the speciation and therefore its solubility. The introduction of anti-solvent facilitates the salting-out phenomenon due to the interaction between solute, solvent, and anti-solvent [22, 23].

$$\triangle G = (\mu_2 - \mu_1) = -RT\ln(S) \tag{1}$$

$$S = \frac{Q}{K_{sp}} = \frac{a_A^a a_B^\beta}{K_{sp}} \text{ for } A_a B_\beta \text{ salt} \tag{2}$$
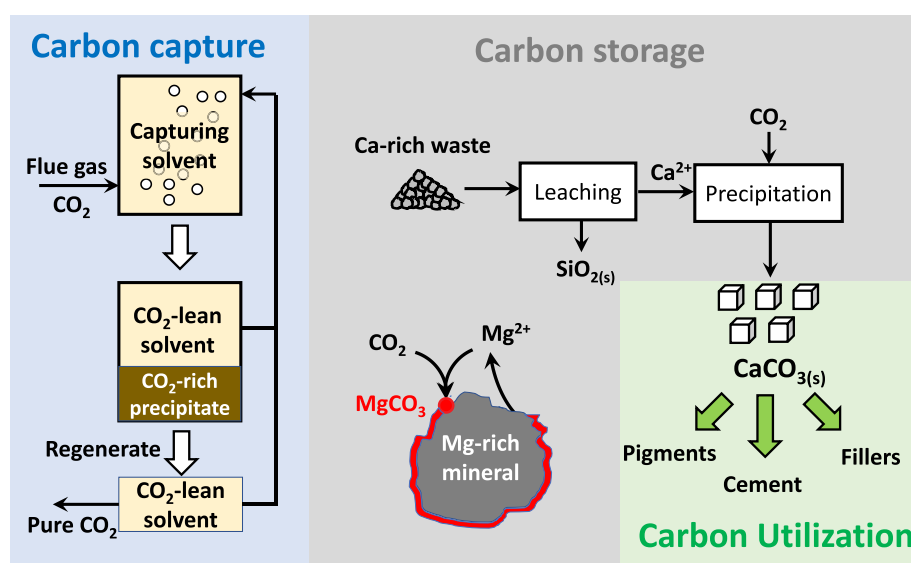
Fig. 1 Framework of this review on the role of chemical precipitation in CCUS

Lin *et al. Sustainable Environment Research* (2022) 32:45

Page 3 of 20

Fig. 2 **a** Solubility products of different polymorphs of calcium carbonate at different temperature [21]. **b** Gibbs free energy of nucleation as a function of radius of spherical nucleus (Assume that the molecular volume (v) = 5 × 10⁻²⁹ m³, interfacial energy of cluster-water (γ_{CW}) = 0.5 J m.⁻², and that heterogeneous nucleation reduces surface energy by 40%). **c** Dissolution rate of Ca-rich and Mg-rich silicate minerals [24, 25]

The classical nucleation theory states that the homogeneous nucleation rate is related to the frequency of effective collision and the ratio of activation energy of nucleus formation (ΔG^*, J) to thermal energy ($k_B T$, J) as shown in Eq. (3) [26]. The Gibbs free energy to form a nucleus from saturated solution is composed by the free energy to form a new volume (ΔG_V, J) and new surface (ΔG_S, J), as shown in Eq. (4). ΔG_V is the products of the number of molecules in the nucleus (j) and the chemical potential difference expressed by S; ΔG_S is describable by the surface area (A, m²) and the interfacial tension of the cluster-water interface (γ_{CW}, J m⁻²) [19]. Provided that the nucleus is spherical, the volume and surface area of nucleus is expressed by its radius r (Eq. (5)). At critical radius r*, ΔG meets a maximum as the activation energy for nucleation. Once the nucleus becomes larger than r*, its further growth is favored. Equation (6) shows the ΔG^* and r* of spherical nucleus, which decrease with greater S as shown in Fig. 2b. In the case of heterogeneous nucleation, the surface free energy is revised as Eq. (7) to account for the substitution of substrate-water interface by substrate-cluster interface. If the γ_{CS} approaches zero and γ_{SW} is similar to γ_{CW}, ΔG_S would be reduced to $\gamma_{CW}(A_{CW} - A_{CS})$, suggesting that the activation energy of heterogeneous nucleation can be lower than homogeneous nucleation. When the supersaturation is too low for nucleation, crystal growth could take place and its rate is related to the supersaturation, depending on the rate-limiting step [27].

$$J = \overline{A}\exp\left(\frac{-\Delta G*}{k_B T}\right) \qquad (3)$$

$$\Delta G = \Delta G_V + \Delta G_S = -jk_B T\ln S + \gamma_{CW}A \qquad (4)$$

$$\Delta G = -\frac{4\pi}{3v}r^3 k_B T \ln S + 4\pi r^2\gamma \qquad (5)$$

$$\Delta G^* = \frac{16\pi v^2 \gamma_{CW}^3}{3k_B^2 T^2(\ln S)^2} \text{ at } r^* = \frac{2\gamma_{CW}v}{k_B T \ln S} \qquad (6)$$

$$\Delta G_S = \gamma_{CW}A_{CW} + (\gamma_{CS} - \gamma_{SW})A_{CS} \qquad (7)$$

where Ā is the frequency of effective collision (s⁻¹), ΔG is the Gibbs free energy (J) of a nucleus with a radius of r (m), ΔG^* is the activation energy (J) at critical radius of r* (m), ΔG_V is the volume free energy (J), ΔG_S is the surface free energy (J). j is the number of molecules in a nucleus, v is the molecular volume (m³), γ_{CW}, γ_{CS}, and γ_{SW} are the interfacial energy of cluster-water, cluster–substrate, and substrate-water interface (J m⁻²), S is

Lin *et al. Sustainable Environment Research* (2022) 32:45

Page 4 of 20

the supersaturation ratio, k_B is the Boltzmann constant (1.38×10^{-23} m^2 kg s^{-2} K^{-1}), and T is temperature (K).

The dissolution rate of minerals depends on the concentration of surface groups. For example, the silicate surface can be protonated, deprotonated, or chelated by ligands. Therefore, the dissolution rate is related to specific surface area, pH, ligand concentration, and the degree of hydration in supercritical CO$_2$ (scCO$_2$) [28]. Figure 2c depicts the dissolution rate of various Ca-rich and Mg-rich silicates that are potential feedstocks for mineral carbonation. When the silica nucleates on the surface of silicates, the overall dissolution rate would decrease since the surface is occupied. Dissolution plays an important role in phase transformation of the precipitate from metastable to stable phase, as will be shown in the phase transformation of calcium carbonate.

3 CO$_2$ capture by precipitation-incorporated solvent

The absorption of CO$_2$ by regenerable solvent is an effective approach to post-combustion decarbonation and produce concentrated CO$_2$ stream for sequestration. However, the high demand of energy in regenerating solvent after the capture of CO$_2$ is the bottleneck of the process [29]. Take the most common absorbent – monoethanolamine (MEA) as an example, its regeneration energy is around 3.2–4.0 MJ per kg of captured CO$_2$ [30]. One of the strategies to reduce the energy penalty of carbon capture is to use a phase change solvent that undergoes phase transition after CO$_2$ absorption, forming a CO$_2$-lean liquid phase and a CO$_2$-rich liquid or solid phase [12]. Since only the CO$_2$-rich phase requires regeneration, the energy demand of CO$_2$ capture can be minimized. In this section, we will summarize the development of CO$_2$ capture solvents that involve liquid–solid phase change after CO$_2$ absorption, including amine, ammonia, and amino acid.

3.1 Amine-based solvent

The regeneration of the aqueous amine solution is hampering the large implementation of CO$_2$ capture. When the solvent is changed to a mixture of water and alcohols, phase separation may occur, in which the upper liquid phase is lean in CO$_2$ and can be reused for CO$_2$ capture without regeneration. Li et al. [31] investigated the CO$_2$ capture by MEA, N-Methyldiethanolamine (MDEA), diethylenetriamine (DETA), and triethylenetetramine (TETA) in alcohol solution. Whether the precipitation would occur depends upon the composition of solvent and the structure of amines. As shown in Fig. 3a, the difference between the solvation energy of DETA carbamate in water and alcohol was the greatest, indicating that the prominent solubility difference. Therefore,
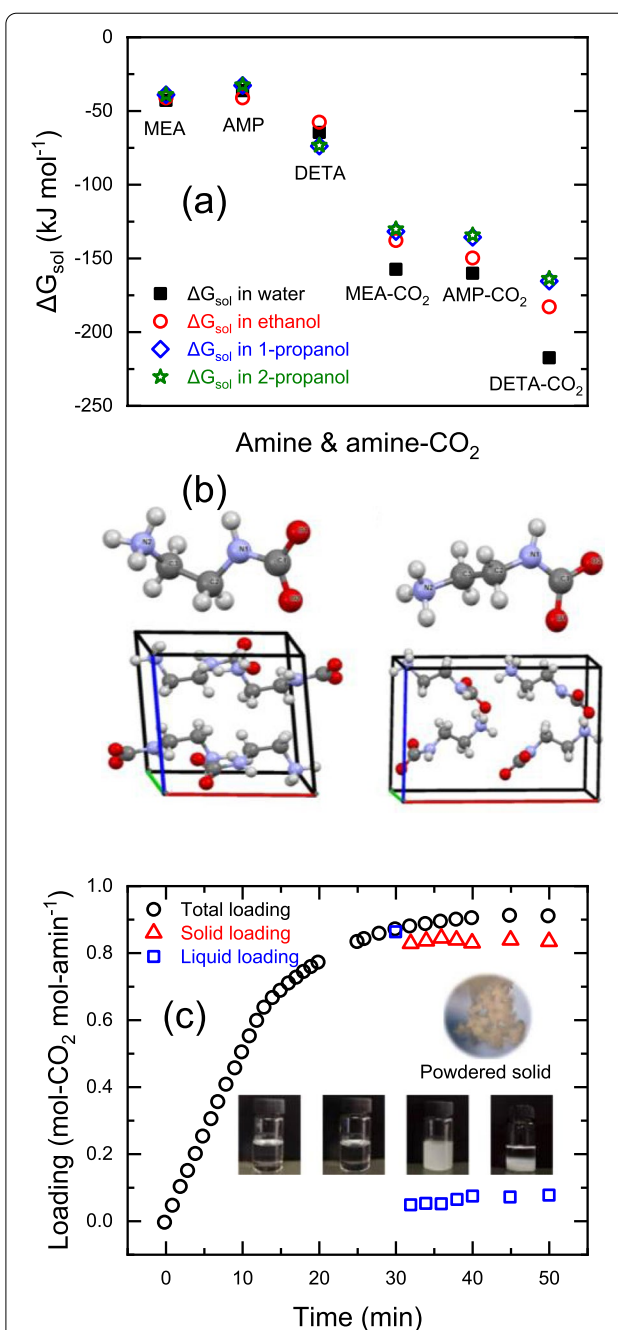
Fig. 3 **a** Variation in solvation free energy (ΔG_{sol}) of selected amines in different solvents (Reproduced from [31] with permission from Elsevier). **b** Crystal structure of monoclinic and orthohombic EDA-carbamate formed in DMF solution and DMA solution, respectively (Reprinted from [32] with permission from Elsevier). **c** Precipitation behavior of TETA/AMP in NMP upon CO$_2$ absorption (Reproduced from [33] with permission from Elsevier)

the precipitation of DETA carbamate took place when the ratio of 1-propanol increased to 60%. Li et al. [32] reported that the crystal structure of the precipitated carbamate is related to the solvent composition. As shown
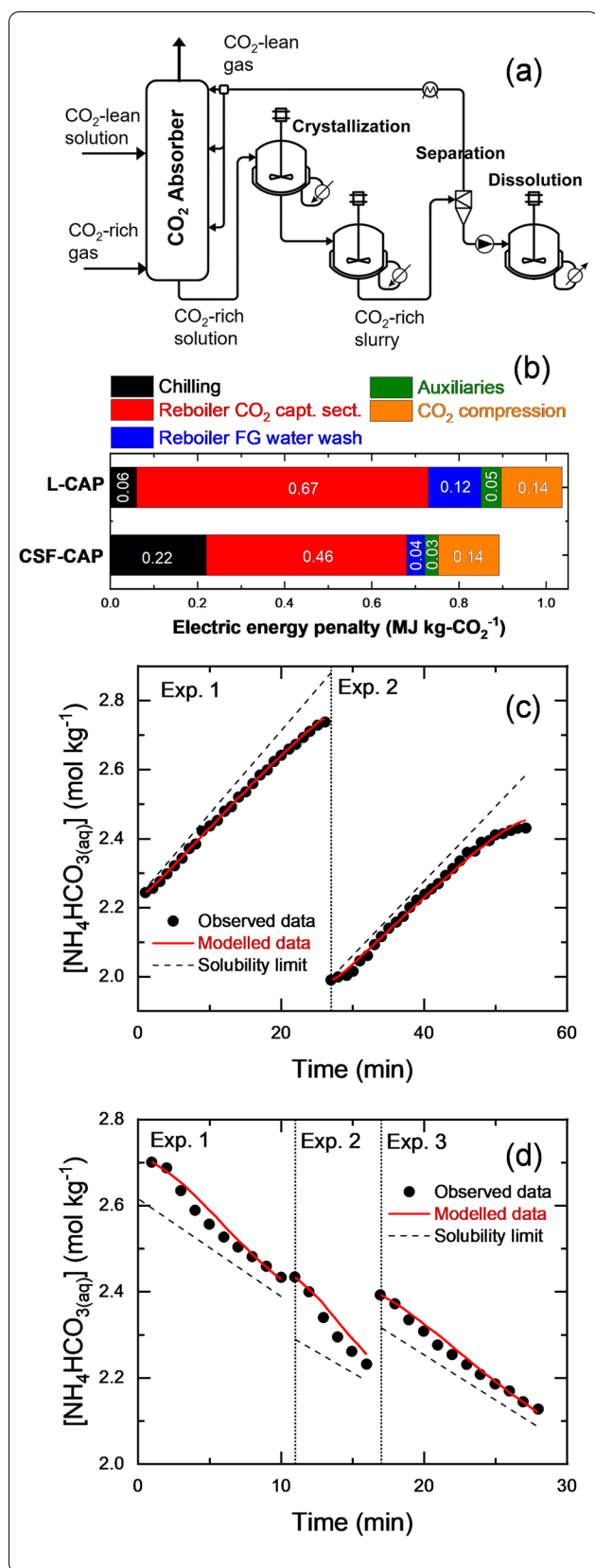
Fig. 4 a Flow diagram of the chilled-ammonia process involving the precipitation process. **b** Estimated energy penalty of chilled-ammonia process excluding precipitation (L-CAP) and involving precipitation (CSF-CAP) (Reproduced from [36] with permission from The Royal Society of Chemistry). **c** Crystal growth rate and **d** dissolution rate of ammonium bicarbonate at different concentration of ammonia (Reproduced with permission from [37]. Copyright 2019 American Chemical Society)

in Fig. 3b, the precipitated carbamate of 1,2-ethanedi-amine (EDA) was monoclinic and orthorhombic in N,N-dimethylformamide (DMF) and N,N-dimethylacetamide (DMA), respectively. The heat duty of the regeneration of the EDA-carbamate would be different as the decomposition monoclinic and orthorhombic EDA-carbamate took place at 136 and 151 °C with regeneration energy of 134 and 188 kJ mol^{-1}, respectively.

The precipitation of TETA for CO_2 capture was explored in non-aqueous system. Liu et al. [34] elucidated the role of ethanol in the absorption of TETA. The higher solubility of CO_2 in ethanol than in water resulted in a much greater absorption rate. Around 80% of the absorbed CO_2 ended up as the precipitate of TETA-carbamate. The predominance of ethyl carbonate ($C_2H_5OCO^{2-}$) in ethanol solvent could be regenerated more efficiently than the carbamate ions [34]. Gao et al. [33] adopted the density function theory and molecular dynamic simulations to study the phase transition of the TETA/2-amino-2-methyl-1-propanol (AMP) in N-methylformamide (NMP). The capture of CO_2 involved the formation of zwitterion (TETA$^+CO_2^-$ and AMP$^+CO_2^-$) and a series of protonation and deprotonation reactions. The strength of hydrogen bonding and Van der Waal interaction dictate the solubility and aggregation of the final product (TETA(H$^+$)$_2$(CO$_2^-$)$_2$) (Fig. 3c).

3.2 Chilled-ammonia process
To circumvent the problems of conventional amine solvent, such as high cost, equipment corrosion, and amine degradation, the use of ammonia as an CO_2 absorbent was developed and patented as the chilled ammonia process (CAP) [35]. The absorption of CO_2 by the ammonia was facilitated between 5–15 °C. The capture solution is regenerated at higher temperature (50 to 200 °C) and moderate pressure (200 kPa to 13.6 MPa). While the system can be operated below the saturation of ammonium bicarbonate as non-solid CAP process, Sutter et al. [36] reported that the controlled-solid formation CAP process (Fig. 4a). Compared to the CAP that excludes precipitation, the controlled-solid formation CAP could decrease the steam demand for CO_2 desorption by 30% and the specific primary energy consumption for CO_2 avoided by 17%. As shown in Fig. 4b, the energy efficiency lies in

the lower energy demand for the regeneration through crystal dissolution. Milella and Mazzotti [37] studied the kinetics of the crystallization and dissolution of ammonium bicarbonate in depth. The rate constants of crystal growth and dissolution were acquired at $S \leq 0.15$ and $S \geq -0.05$, respectively. Accordingly, the established model managed to predict the rates of crystal growth and dissolution (Fig. 4c and d), and variation in the concentration of nitrogen and carbon species.

3.3 Amino acid-based solvent

Another alternative solvent for CO_2 capture being investigated is amino acid salts. The amino functional group grants the amino acid salts their superior performance than the conventional alkanoamines. The advantages of amino acid salts include negligible volatility, higher stability and resistance, and low environmental impact [38, 39]. The counter ion of the amino acid salts affects not only the CO_2 absorption capacity, but reaction rate. In most cases, potassium amino acid salts outperform the ones with sodium and lithium ion [40, 41]. The high concentration of amino acid salts and large CO_2 loading may lead to the precipitation of amino acid, carbamate, and bicarbonate upon the decrease of pH in CO_2 absorption. The type of precipitate depends on the structure and solubility of the amino acid [38]. For example, amino acids are the preferred precipitate when primary amino acids are used; bicarbonate salts may form for the amino acids with more steric hindrance; carbamates may appear when amino acid salts are used with amine-based absorbent [38, 42].

Sanchez-Fernandez et al. [38] reported the use of potassium taurate to capture the CO_2 from flue gas with through precipitation, denoted as DECAB process. The precipitation of tauric amino acid in the spray tower was driven by the change in pH. Compared to the conventional MEA absorption system, the energy required for DECAB to regenerate the absorbent decreased by 10% because less heat is required for the dissolution of amino acid. To further improve the energy efficiency, the DECAB-plus process was developed by regenerating only the thick slurry and recycling the supernatant directly to the spray tower, whose flow diagram is presented in Fig. 5a. By doing so, the reboiler duty per ton of CO_2 can be decreased by 30% [43]. As shown in Fig. 5b, DECAB and DECAB-plus are compared with the pH-swing and conventional MEA capture technology in several aspects. The DECAB processes showed low environmental impact, corrosion, and energy consumption than the MEA system. However, the low absorption flux is susceptible to increase the capital expenditure [43].

The precipitation of amino acid salts can be triggered by the antisolvent precipitation. Alivand et al. [44]

demonstrated that the potassium glycinate dissolved in DMF/water solution produced carbamate and bicarbonate precipitate upon CO_2 capture (Fig. 5c). DMF behaved as an antisolvent that diminished the solubility of the carbon-rich solids, including carbamide and potassium bicarbonate. An optimal DMF content of 60% was concluded to produce the greater portion of CO_2-lean supernatant and provide an absorption capacity of 0.55 mol CO_2 per mol of potassium glycinate. Chen et al. [45] studied the precipitation of CO_2-loaded potassium glycinate by the addition of ethanol. Solid–liquid-liquid phase separation was observed upon the dosing of ethanol. The main composition of the solid phase was glycine, carbamate, and potassium bicarbonate. The upper liquid phase was ethanol solution, and the lower liquid phase was a mixture of glycine, glycinate, and bicarbonate. More than 90% of the glycine was precipitated with the addition of ethanol at volume ratio of 1.6, which can minimize the energy required for regeneration.

4 CO_2 storage by mineral carbonation

Mineral carbonation is a geochemical process that stabilizes the CO_2 through the formation of carbonate minerals with metal cations, such as Ca^{2+}, Mg^{2+}, or Fe^{2+} [46].

The feedstocks vary from naturally-occurring minerals, mining tailings, to industrial wastes. Since the end products of carbonation are thermodynamically stable, they can be reutilized or stored above ground without constant monitoring [46, 47]. Mineral carbonation can be in-situ or ex-situ [46] as illustrated in Fig. 6a. In the case of in-situ mineral carbonation, the CO_2 for storage is captured from the post-combustion stream in off-site facilities, which is compressed and injected into a geologic sink where the host rocks can react with CO_2 to form carbonates [48]. Therefore, the direct geochemical reactions between pressurized CO_2 and minerals are studied to resemble the in-situ mineral carbonation. On the other hand, ex-situ carbonation is performed in a reactor using captured CO_2 or flue gas, where the solid feedstocks are carbonized through direct or indirect process [46]. The direct carbonation is a single-step reaction, in which the feedstocks react directly with CO_2, as shown Fig. 6b. Since the direct carbonation facilitates the metal dissolution and carbonate precipitation at the same time, the reaction rate is often compromised [46]. In contrast, the indirect carbonation divides the process into multiple steps to accelerate and optimize the carbonation process (Fig. 6c). The steps include the extraction of metal from feedstocks, the conversion of metal into metal hydroxide, and the precipitation of CO_2 using metal hydroxide as carbonates [49]. In this section, the precipitation of carbonate minerals is discussed based on the feedstocks,
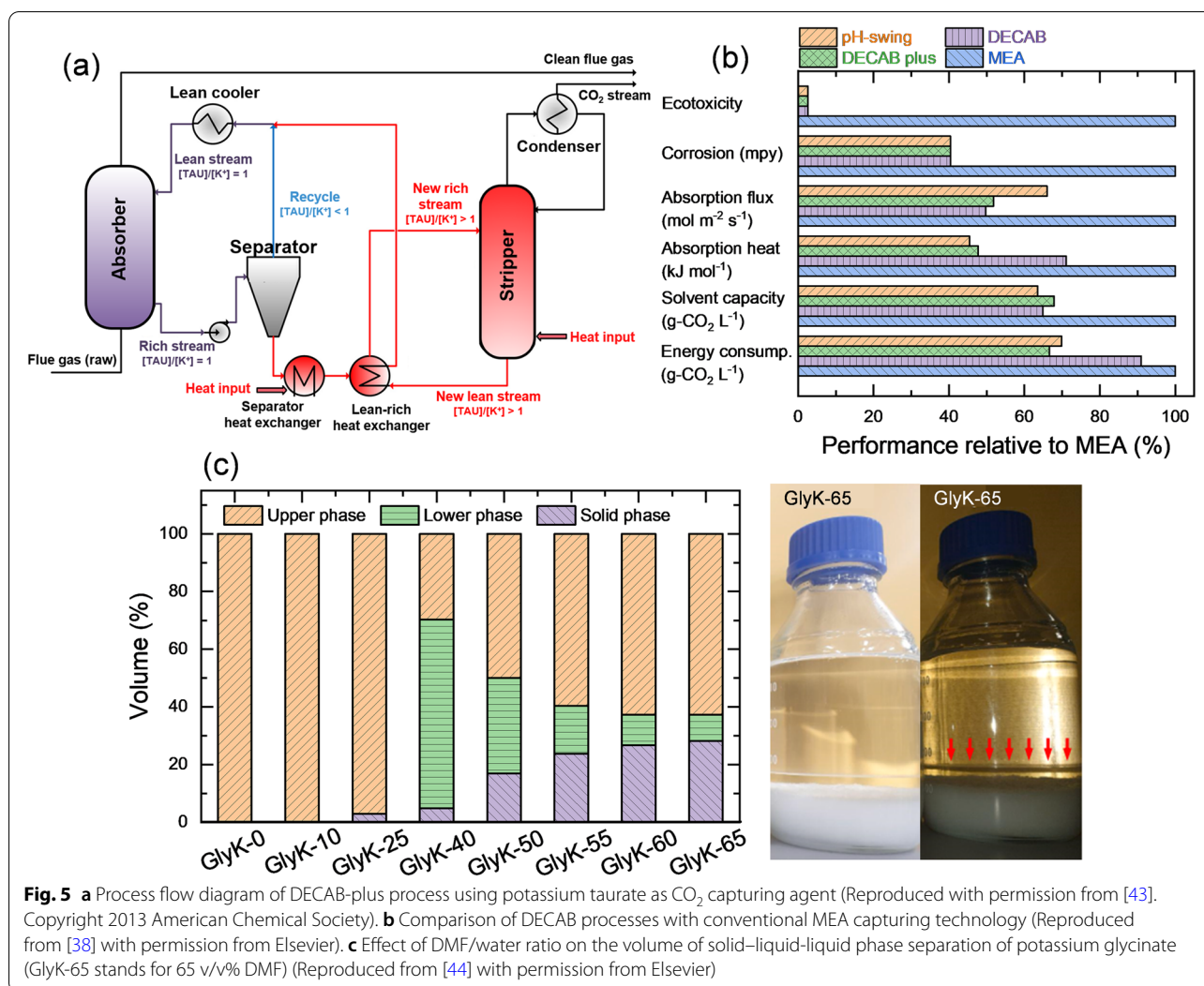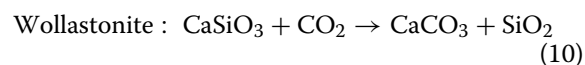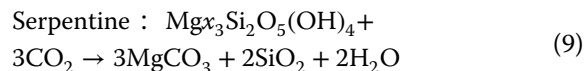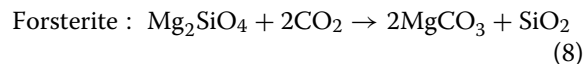
Fig. 5 a Process flow diagram of DECAB-plus process using potassium taurate as CO_2 capturing agent (Reproduced with permission from [43]. Copyright 2013 American Chemical Society). **b** Comparison of DECAB processes with conventional MEA capturing technology (Reproduced from [38] with permission from Elsevier). **c** Effect of DMF/water ratio on the volume of solid–liquid-liquid phase separation of potassium glycinate (GlyK-65 stands for 65 v/v% DMF) (Reproduced from [44] with permission from Elsevier)

including nature minerals, mining wastes, and industrial wastes.

4.1 Silicate minerals

Silicate minerals are abundant materials that can capture CO_2 into solid carbonates naturally. Magnesium and calcium are commonly present in silicate minerals, rendering them great potential in carbonation [11]. The magnesium silicates that are abundant in the crust include olivine $((Mg,Fe)_2SiO_4)$, forsterite (Mg_2SiO_4), and serpentine $(Mg_3Si_2O_5(OH)_4)$. Wollastonite $(CaSiO_3)$ is representative for the carbonation of calcium-rich silicate. The carbonation of olivine, forsterite, serpentine, and wollastonite into magnesite $(MgCO_3)$ or calcite $(CaCO_3)$ and silica (SiO_2) follow Eqs. (8)- (10), respectively [50]. The direct carbonation of the silicates was studied to simulate the subsurface

carbonation using pressurized CO_2, either in sub-critical or supercritical condition.

$$\text{Forsterite}:\ Mg_2SiO_4 + 2CO_2 \rightarrow 2MgCO_3 + SiO_2 \tag{8}$$

$$\text{Serpentine}:\ Mgx_3Si_2O_5(OH)_4 + 3CO_2 \rightarrow 3MgCO_3 + 2SiO_2 + 2H_2O \tag{9}$$

$$\text{Wollastonite}:\ CaSiO_3 + CO_2 \rightarrow CaCO_3 + SiO_2 \tag{10}$$

Considering that the CO_2 injected to subsurface is in supercritical phase (T > 31 °C, P > 7.4 MPa) [51], the interaction between silicates, $scCO_2$ and brine has been studied extensively. The water content in the $scCO_2$ influences the dissolution of silicates, mass transfer, and the precipitation of carbonates, which influence the overall carbonation efficiency. Kwak et al. [52] investigated the
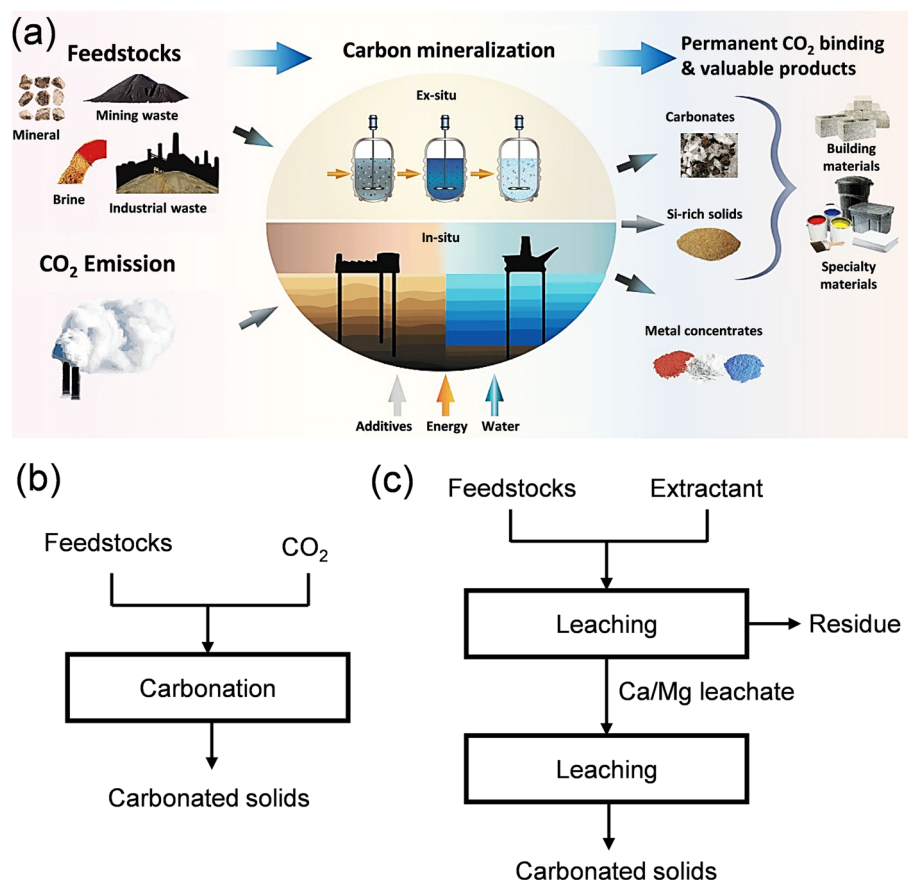
Fig. 6 a Carbon mineralization from various feedstocks to different products. Image courtesy of Florent Bourgeois, Laboratoire de Génie Chimique; Au-Hung Park and Xiaozhou Sean Zhou, Columbia University. Process flow charts of **b** direct and **c** indirect carbonation
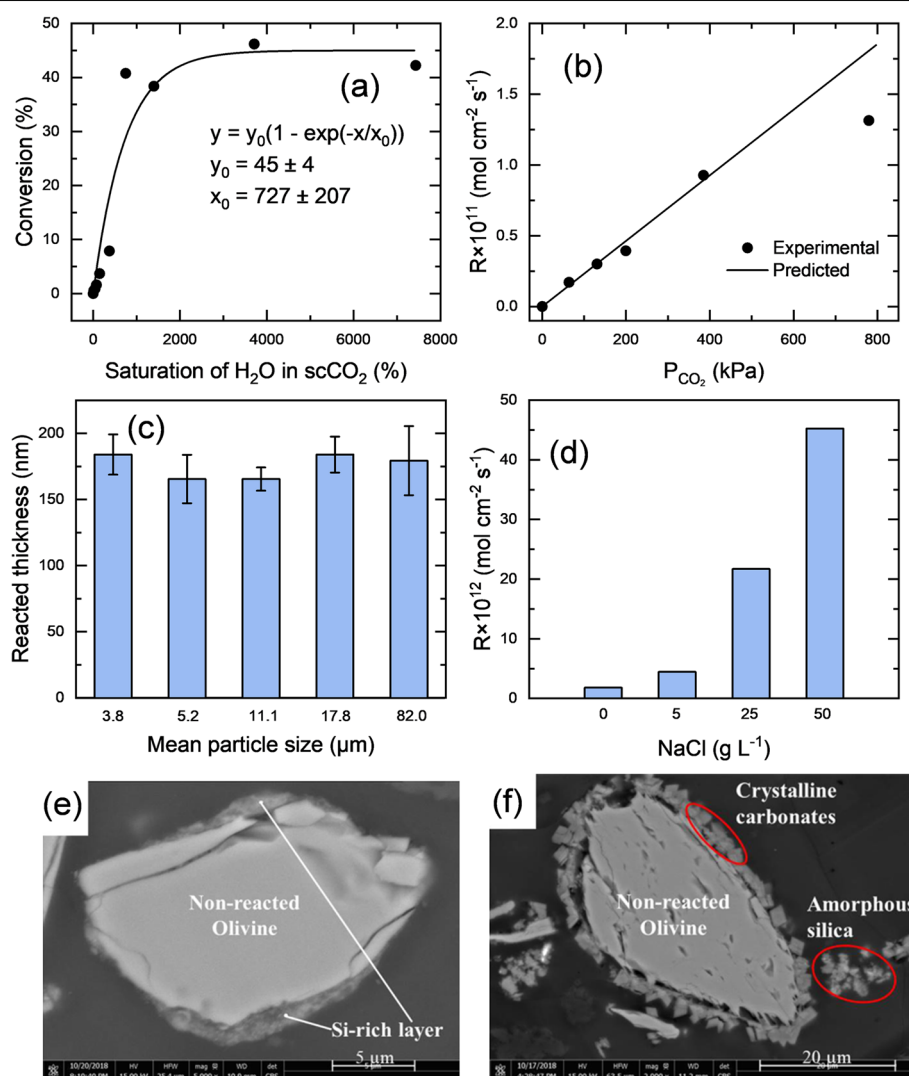
effect of initial water content in $scCO_2$ on the direct carbonation of forsterite. When the water content in $scCO_2$ is below saturation, less than 2% of forsterite was reacted. In contrast, the presence of excessive water (20-fold of the saturation value) in $scCO_2$ significantly promoted the extent of reaction to 45%, as shown in Fig. 7a. Placencia-Gómez et al. [53] elucidated the role of water film that adsorbed on the surface of forsterite using Fourier transform infrared and electrical impedance spectroscopy. The threshold water coverage was estimated to be 1.5 monolayers, in which the dissolution and mass transport are promoted. This was also seen in the study conducted by Loring et al. [54] on forsterite carbonation in $scCO_2$ where at 95 and 136% water saturation, about 2 and 10% conversion, respectively were achieved at 50 °C and 18 MPa for 24 h.

Temperature and pressure determine the equilibrium solubility, reaction rate and activity of carbonate species. Wang et al. [58] investigated the effect of temperature and partial pressure of CO_2 on the direct carbonation of olivine. The activation energy was found independent of particle size, being 50 kJ mol^{-1}. At 3.4 MPa, the carbonation efficiency was maximized at 175 °C while a further increase temperature impaired the efficiency [58]. The phenomenon is attributed to the decreased activity of bicarbonate at higher temperature when the pressure is constant [59]. Felmy et al. [60] conducted a study to prove that even at low temperatures, forsterite is capable of CO_2 sequestration through direct carbonation. Results showed that at relatively low temperatures (30–50 °C), forsterite first produced hydrated with water-saturated $scCO_2$ produced magnesite ($MgCO_3$) and amorphous silica phase after 14 d. On the other hand, the pressure of CO_2 regulates the concentration of dissolved inorganic carbonate, which dominated the dissolution rate of divalent ion from silicates. As shown in Fig. 7b, the dissolution rate of magnesium ion from heat-treated serpentine increased linearly with the partial pressure of CO_2 [55].

The pretreatment of natural silicates can enhance the reactivity toward carbonation through mechanical and thermal routes. The thermal activation of serpentine enhances its carbonation efficiency by the

Fig. 7 a Effect of water content in scCO$_2$ on the conversion of forsterite (Mg$_2$SiO$_4$) (Reproduced from [52] with permission from Elsevier). **b** The increase in partial pressure accelerated the initial dissolution rate of Mg^{2+} from heat-treated serpentine (Reproduced with permission from [55]. Copyright 2014 American Chemical Society). **c** The thickness of reacted wollastonite in scCO$_2$ (Reproduced with permission from [56]. Copyright 2017 American Chemical Society). **d** Effect of sodium chloride concentration on the dissolution rate of forsterite (Reproduced with permission from [57]. Copyright 2013 American Chemical Society). SEM photo of olivine carbonized in scCO$_2$ **e** without any addition of salt and **f** with 1.05 M NaCl and 1.05 M NaHCO$_3$ (Adapted from [58] with permission from Elsevier)

dehydroxylation reaction that liberates structurally bound hydroxyl groups, producing forsterite (Mg$_2$SiO$_4$) and enstatite (MgSiO$_3$) [61]. The limiting reaction in the direct mineralization is the dissolution of divalent ions, which takes place at solid–liquid interface. The mechanical treatment can reduce the particle size to produce more surface for dissolution. Min et al. [56] investigated the direct carbonation of wollastonite with different particle size (3.8–82 µm) in water-bearing scCO$_2$ at 60 °C and 10 MPa for 40 h. Regardless of the particle size, the thickness of reacted wollastonite layer was found to be

180 nm, as depicted in Fig. 7c. In other words, the carbonation capacity is correlated with the available surface area. Similarly, the carbonation efficiency of olivine decreased from 66 to 10% as the particle size range increased from 0–25 to 53–75 µm [58]. The leachability of Mg^{2+} from thermally activated serpentine is correlated with its particle size. Du Breuil et al. [62] reported that the comminution of serpentine prior to thermal treatment could improve the magnesium leachability by 4 times, compared to the ones activated unpulverized.

Table 1 Composition of the industrial wastes with potential in mineral carbonation

Chemical composition (%)	CaO	MgO	SiO$_2$	Al$_2$O$_3$	Fe$_2$O$_3$	Ref.
Fly ash (bituminous coal)	1–12	0–5	20–60	5–35	10–40	[72]
Fly ash (sub-bituminous coal)	5–30	1–6	40–60	20–30	4–10	[72]
Fly ash (lignite)	15–40	3–10	15–45	10–25	4–15	[72]
Blast furnace slag	29–50	0–19	30–40	7–18	0.1–1.5	[73]
Steel slag	30–50	5–12	10–20	1–10	3–30	[74]
Red mud	0–14	-	5–30	10–22	20–45	[75]
Waste gypsum	30–32	-	1–5	< 1	0–30	[76]

The silica that formed during the direct carbonation of silicates is critical to the efficiency of CO$_2$ sequestration. As heterogeneous nucleation is favored over the homogeneous, silica is preferred to deposit on the surface of silicates, passivating the surface and hindering further dissolution of divalent ion. Johnson et al. [63] observed the formation of amorphous SiO$_2$ precipitate as a passivating layer in 2 d, causing the dissolution rate of olivine decreased by 2 orders of magnitude. Therefore, only 7% of olivine was converted to magnesite in 94 d. Min et al. [56] performed the carbonation on the wollastonite possessing a pre-existing layer of silica that was formed in aqueous nitric acid solution. Surprisingly, the pre-existing layer of silica did not hamper the carbonation of wollastonite. The result suggests that the porosity of the silica layer formed in water-bearing scCO$_2$ is denser and less porous than the silica formed in aqueous phase. The salinity was found influential on the passivation of silica. Johnson et al. [63] reported that the presence of 0.5 M NaCl affected the dissolution rate of olivine during the direct carbonation. Based on the dissolution of Mg and Si, the authors identified two kinetic regions of dissolution. In the first 5 d of fast dissolution region, more olivine was dissolved in the electrolyte-free condition than in high saline condition. However, the presence of 0.5 M NaCl increased the long-term dissolution rate (> 5 d) by a factor of 5. The phenomenon is attributed to the modified electrical double layer due to the presence of sodium ion, which altered the nucleation mechanism of silica. In several studies of statistic modelling, the increased salinity was found beneficial to the rate of carbonation [56, 64, 65]. The carbonated olivine showed great difference upon whether additional salt was present. As shown in Fig. 7e and f, the direct carbonation of olivine without any salinity led to a dense layer of silica shell. In the presence of 1.05 M NaHCO$_3$ and 1.05 M NaCl, the silica did not deposit on the surface of olivine but form as aggregates [58]. The cause of the dissolution promotion is attributable to the enhanced dissolution rate of silica, the local

enrichment of Na$^+$ in the vicinity of silicate surface, and the change in the activity coefficient [57, 66].

To circumvent the slow kinetics of direct carbonation, the silicate feedstocks can be carbonized directly. Turri et al. [67] developed a process to carbonize olivine through a series of processes, including flotation separation, acid dissolution, nickel ion separation, and selective carbonation and separation of products. Results showed that the indirect carbonation achieved higher carbonation efficiency (81%) than the conventional direct process. In addition, the by-products produced in the indirect carbonation of olivine can be further utilized. The silica produced in the acid-dissolution of olivine in sulfuric acid was of nano-size with a BET surface area greater than 500 m^2 g^{-1} [68]. Raza et al. [69] proposed an economical carbonation process that produces valuable products such as silica and hydromagnesite. The study proposed a multistep sequestration involving dissolution of synthetic forsterite in sulfuric acid. The optimized conditions resulted to more than 90% dissolution of forsterite to magnesium sulfate within 2.5 h. Eventually, more than 95% of magnesium sulfate precipitated to hydromagnesite within 35 min.

4.2 Industrial waste

Industrial wastes containing oxides of calcium and magnesium can be used as alternative feedstocks for mineral carbonation to avoid additional energy and costs for extraction, transport or preparation of minerals [70]. Since the wastes are often already comminuted, the high specific surface area grants them reactive toward carbonation [71]. The downside is that they are less available than naturally-occurring minerals, making the application limited to individual plants [50]. Some of the calcium or magnesium-containing industrial wastes considered for mineral carbonation are coal fly ash, slags, waste gypsums, and bauxite residue, whose chemical composition are shown in Table 1.

The composition of fly ash depends on the types of coal, with CaO and MgO contents varying from 6–40 and

3–10 wt%. respectively [72]. Ukwattage et al. [77] demonstrated that the fly ash can be carbonized in aqueous suspension in pressurized CO_2 atmosphere (3 MPa) and elevated temperature (80 °C). The carbonation capacity and rate are influenced by water-to-solid ratio and temperature, which can be optimized at 30 wt% of solid and 120 °C to sequester 27 g CO_2 per kg of fly ash [77]. The indirect carbonation of fly ash is another approach to not only sequester CO_2 but convert fly ash to reusable products for waste minimization. Hosseini et al. [78] evaluated the indirect carbonation of brown coal ash (CaO content of 16 wt%) using ammonium chloride as a leaching agent to produce calcium chloride solution, which was further used for CO_2 sequestration. The ammonia produced in the leaching process can be used as an absorbing agent for CO_2 during the carbonation reaction, enabling the regeneration of ammonium chloride. The process can fix 170 g CO_2 per kg of fly ash with an operation cost of $60 [78].

Blast furnace and steel slags are produced in the production of steel and iron. Because the slags have high calcium content (32–52% CaO) and are produced in significant quantities, it is estimated that global steelmaking slags could annually store up to 172 Mt of CO_2 worldwide [79]. The blast furnace slag is comprised of akermanite ($Ca_2MgSi_2O_7$) and gehlenite (Ca_2AlSiO_7), which is more suitable for indirect carbonation due to the less reactivity. On the contrary, steel slag is rich in calcium silicates, free CaO and forsterite, rendering them more reactive than blast furnace. Ukwattage et al. [80] studied the direct carbonation of steel slag at different CO_2 pressure, temperature, and liquid-to-solid ratio. The increase in CO_2 pressure could enhance the carbonation rate but resulted in similar carbonation capacity. The Ca extraction efficiency was associated with the water-to-solid ratio. Under the optimum condition, the sequestration of 29 g of CO_2 per kg of steel slag was achieved. Indirect carbonation was adapted as well. Yadav and Mehra [81] investigated the dissolution rate of steel slag and its direct carbonation in ambient atmosphere. The carbonation efficiency was correlated to the size of slags, reaching 70% of carbonation for slag particles between 25–37 μm. Moreover, the dissolution of heavy metals is within the permittable levels even at 90 °C. Chen et al. [82] used pickling and rolling wastewaters to leach out ∼ 10% of calcium from refining slag. As shown in Fig. 8a, the leaching of calcium ion decreased with the liquid-to-solid ratio, which can be described by the pseudo-first order kinetics. The calcium-rich slurry was then injected in a rotating packed-bed reactor to facilitate carbonation process under high gravity condition with various rotating speed. As the centrifugal force improves the mass transfer efficiency of gas–liquid interface, the carbonation was realized without the pre-capture of CO_2. Figure 8b shows that the carbonation efficiency increased with gravity factor (β, the ratio of centrifugal force to gravity) until it reached 235, enabling to sequestrate 0.2 g CO_2 per kg of slag [82]. Chu et al. [83] developed an indirect carbonation process for blast furnace slag. The sulfuric acid and ammonia that were used for the leaching and carbonation processes could be produced in an electrolytic cell, minimizing the overall cost. The developed process managed to sequester 361 g CO_2 per kg of blast furnace slags.

The basicity of the by-product of flue gas desulfurization renders its potential in mineral carbonation. Gypsum ($CaSO_4 \cdot 2H_2O$) is a major industrial product produced in wet flue gas desulfurization [76]. The high leachability of calcium from gypsum makes it ideal for carbon sequestration, direct or indirect. Since wet desulfurization-derived gypsum is close to the CO_2-rich flue gas, it is preferred to be carbonized directly using ammonia as the CO_2 absorber. Considering that the temperature of the emitted flue gas is between 50–80 °C, Tan et al. [85] investigated the direct carbonation of desulfurization-derived gypsum in ammonia solution at elevated temperature (40–80 °C). Nearly all the gypsum can be utilized at ammonia-to-gypsum ratio of 2. Song et al. [86] reported that the direct gypsum carbonation in ammonia solution at ambient condition can produce calcium carbonate with high purity. The authors observed the calcium concentration could reach 80 mM before the nucleation of calcium carbonate. Therefore, the filtrate separated before nucleation can be collected to obtain calcium carbonate with high purity. The addition of polyacrylic acid hindered the nucleation of calcium carbonate, which prolonged the induction time and enhanced the dissolved calcium carbonate level (Fig. 8c). As a result, more calcium carbonate was obtained with the addition of 2.7 g L^{-1} polyacrylic acid (Fig. 8d) [84]. For the semi-dry desulfurization process, the by-produced ash is consisted of CaO, $CaCO_3$, $CaSO_4$, and $CaSO_3$ [87]. Du et al. [87] investigated the real-time direct carbonation of semi-dry desulfurization waste at atmospheric pressure and identified three distinct stage based on CO_2 absorption efficiency and carbonation efficiency. By applying the kinetic models of heterogeneous reactions, the authors suggested that the carbonation reaction was limited by film diffusion of CO_2, chemical reaction, and then the diffusion in product layer. Therefore, the process was optimized at 60 °C, 100 g L^{-1}, 400 rpm, and gas flowrate (15% CO_2) of 300 mL min^{-1}, which sequestrated 90% of CO_2 in 4 h [88]. Ragipani et al. [89] reported that the direct mineral carbonation of semi-dry flue gas desulfurization fly ash not only captured and sequestered CO_2 but also reduced the content of sulfur in the fly ash to comply with the requirement of supplementary
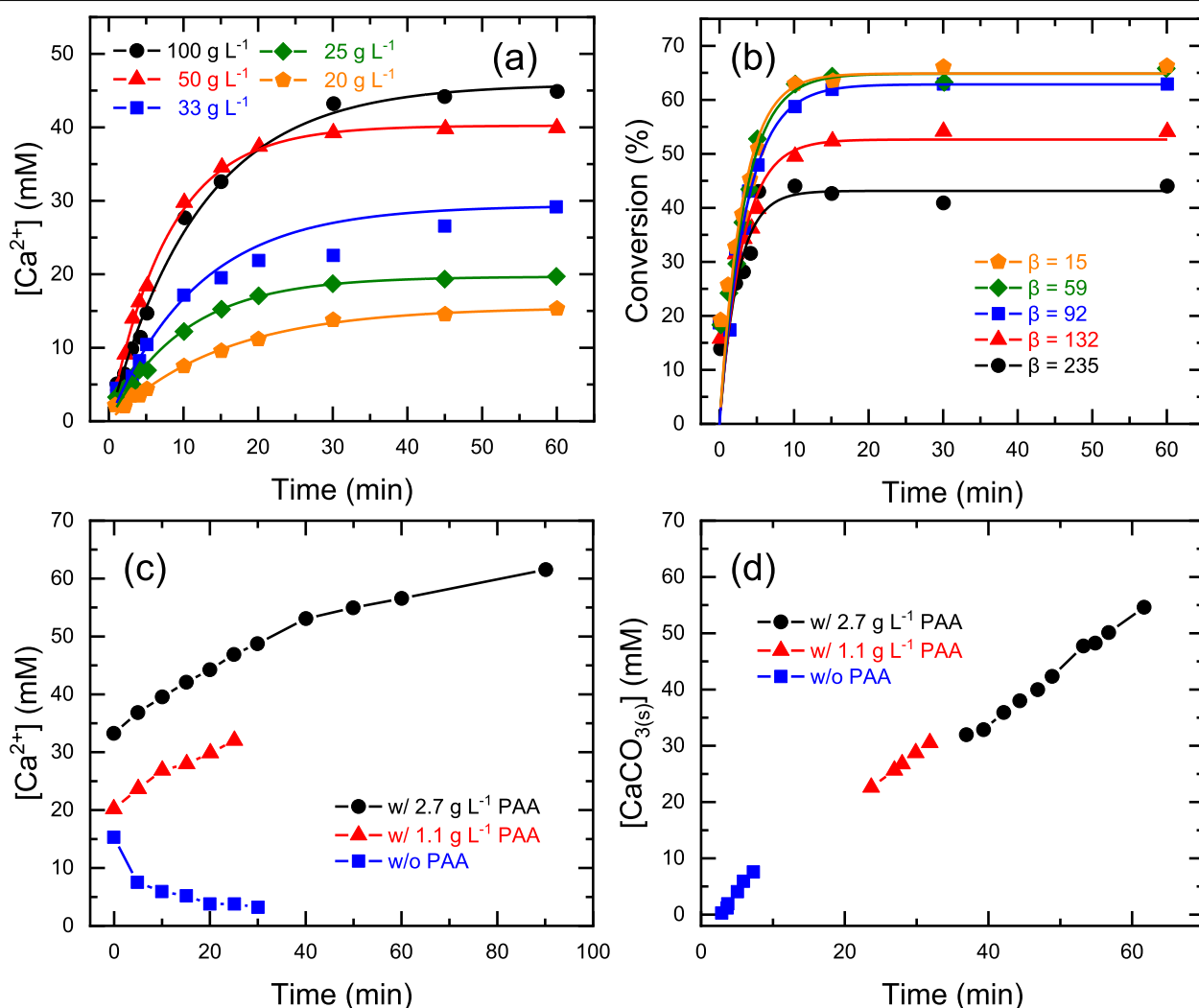
Fig. 8 a Dissolution of calcium from steel slag by cold rolling wastewater as a function of liquid-to-solid ratio (LSR) and **b** its carbonation conversion in rotating packed-bed reactor with various gravity factor (Reproduced from with permission from [82]. Copyright 2020 American Chemical Society). Effect of polyacrylic acid on **c** dissolution behavior of waste gypsum and **d** amount of pure calcium carbonate formation (Reproduced from [84] with permission from Elsevier)

cementitious materials (total sulfur content < 5.0%) [89]. Upon pressurizing in CO_2 atmosphere, the sulfur content of the fly ash was extracted by the dissolution of calcium sulfite through the neutralization of dissolved CO_2. Therefore, the total sulfur content was eliminated from 10.4 to 4.9 wt% by direct carbonation of fly ash at 500 kPa of CO_2 atmosphere with a solid-to-liquid ratio of 20 g L^{-1}, which sequestrated CO_2 was estimated to be 17.3 g per kg of ash [89].

The by-product of mining waste are potential feedstocks of mineral carbonation, including red mud, limestone mine waste, and magnesium-rich tailings. The production of alumina from bauxite produces red mud, a highly alkaline residue that contains oxides of aluminum,

calcium, silicon and iron [90]. The carbonation of red mud is regarded to be an inexpensive and safe process, producing of thermodynamically stable carbonates and eliminating environmental and health hazards of red mud [91]. Yadav et al. [92] used red mud samples of varying size fractions based on density via aqueous carbonation. It was found that the mineral phases responsible for the carbonation of red mud are the calcium-bearing cancrinite and chantalite. A layer of calcite was identified after carbonation, resulting in a carbonation capacity of red mud of 53 g CO_2 per kg of red mud. Kashefi et al. [93] explored the indirect carbonation of red mud that involved an ex-situ multistep pH-swing process to recover silica, iron hydroxide, and aluminum hydroxide from the leachate.

The process extracted 85% calcium from the red mud at 80 °C within 2 h using 1 M HCl. Calcium carbonate with 98% purity was ultimately obtained and the carbonation capacity was 34 g CO_2 per kg of red mud. The carbon sequestration by limestone mining waste that is rich in calcium and magnesium oxides (>70 wt%) was investigated [94–96]. Besides calcite and magnesite, the calcium and magnesium silicates were also the constitutes of limestone mining waste that can be utilized for mineral carbonation [95]. The authors performed the direct mineral carbonation of limestone waste in ambient condition at pH 10 in ambient condition, which achieved a carbonation efficiency of 5.3% in 24 h. Since the direct carbonation is controlled by surface reaction, the carbonation efficiency of the fine limestone waste (<38 μm) was 15% greater than the coarse one (<75 μm) [96]. The tailings of chrysotile, ultramafic and mafic rocks are ideal for carbon sequestration considering the abundance of magnesium-containing minerals [97]. Oskierski et al. [98] assessed the carbonation capacity of a mine tailings of a closed asbestos mine in New South Wales, Australia. It was estimated that about 70 kt CO_2 had been sequestered by the above-ground mine tailings pile, carbonating them into hydromagnesite ($Mg_5(CO_3)_4(OH)_2 \cdot 4H_2O$) and pyroaurite ($Mg_6Fe_2CO_3(OH)_{16} \cdot 4H_2O$), since its closure 29 years ago. The passive carbonation rate was estimated to be 4.9 kg-CO_2 m^{-2} yr^{-1} [98], which is significantly higher than that of chemical weathering. Power et al. [99] estimated the rate of CO_2 mineralization during carbonation of tailings of Baptiste deposit within the Decar nickel district in British Columbia, Canada. The amount of CO_2 sequestered are related to the supply of the CO_2. The direct air capture could sequester 3.5 kg-CO_2 m^{-2} yr^{-1}, which can be enhanced to 19 kg-CO_2 m^{-2} yr^{-1} with the aid of aeration. The carbonation of the ultramafic tailings with 10% CO_2 gas could potentially fixate 210 kt CO_2 yr^{-1}, offsetting 42–53% of the CO_2 emission of the mine [99].

5 Precipitation of calcium carbonate and its utilization

Calcium carbonate is the main product in the indirect carbonation of industrial waste which could be utilized in various industries [17]. In this section, the factors that control the precipitation of calcium carbonate are summarized in terms of its polymorph. The utilization of the precipitates produced in the indirect carbonation is reviewed.

5.1 Controlled precipitation of calcium carbonate

Depending on the method and condition, calcium carbonate can be amorphous or crystalline. The amorphous calcium carbonate (ACC) generally exists as monohydrated $CaCO_3$ [100] while the polymorphs are usually anhydrous, and further classified as rhombic calcite, needle-like aragonite or spherical vaterite [101]. Calcite is the most stable phase in ambient condition, followed by aragonite and then vaterite [102]. The crystallization of $CaCO_3$ occurs in a series of processes as illustrated in Fig. 9a and b [103, 104]. ACC precipitates first from the supersaturated solution and undergoes the dehydration and recrystallization as vaterite, the least stable polymorph. Lastly, vaterite dissolves and recrystallizes into stable calcite. The scanning electron microscope (SEM) images of the anhydrous polymorphs, vaterite, aragonite and calcite are shown in Fig. 9c to 9e. The differences in polymorphs present in the precipitated $CaCO_3$ lead to differences in physicochemical properties which then dictate potential application [17]. Among the three polymorphs, vaterite is commercially the least significant while calcite is the most commonly used. Aragonite has high length-to-diameter ratio making it suitable for applications requiring strength or incident light scattering [105].

The rate of phase transformation is affected by temperature and pH. Shen et al. [109] revealed that the transformation of ACC to vaterite/calcite is favored between 14 and 30 °C, while the formation of aragonite/calcite is favored between 60 and 80 °C. All the phases coexist at an intermediate temperature range of 40–50 °C [110]. The pH regulates the surface species of calcium carbonate, which governs the rate of dissolution and crystal growth and thus the polymorphs of calcium carbonate [83]. Tai and Chen [111] reported that vaterite was the major product at pH 7.8–12.5 while calcite and aragonite showed up in higher pH at ambient temperature. Nevertheless, the crystallization of aragonite at 7 °C, producing more calcite at pH lower than 11. At 58 °C, nearly pure aragonite was generated at pH below 10. Ramakrishna et al. [112] explored the effect of pH on the synthesis of nano-whisker aragonite. Pure, uniformly-sized (100–200 nm) aragonite needles with high aspect ratio of 30, which can be applied in lightweight plastics, biomedical, pharmaceutical, cosmetic and paint industries. In more alkaline condition, a mixture of calcite and aragonite was obtained.

Aging time affects the extent of phase transformation of calcium carbonate. Luo et al. [113] found that percentage of vaterite first increased with the aging time but decreased after 20 min because vaterite is the intermediate species between ACC and calcite. The manipulation of the aging of calcium carbonate can produce the product with desired property. For example, vaterite has a high specific surface area, great dispersity and lower specific gravity, which is attractive in the applications in personal care [114] and biomedical fields [115]. Jiang et al. [116] synthesized the metastable vaterite with $CaCl_2$ ethanol solution and Na_2CO_3 aqueous solution. The authors
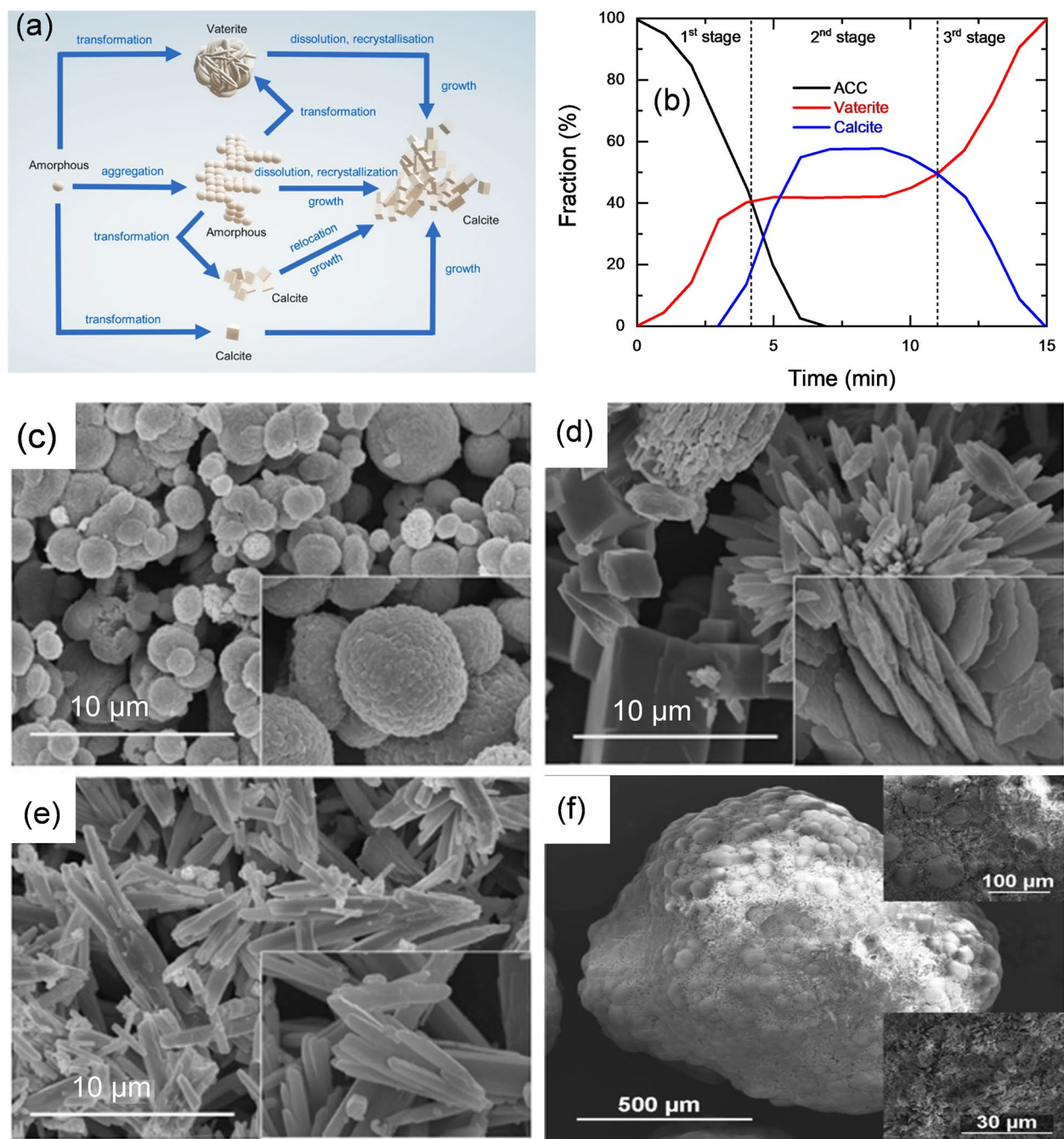
Fig. 9 a Reaction route of the calcium carbonate polymorphs (Adapted from [103] with permission from Elsevier). **b** Evolution of the calcium carbonate polymorphs (Reproduced from [106] with permission from Elsevier). SEM micrographs of **c** spherical vaterite, **d** rosette-shaped aragonite and cubic calcite, **e** needle-like aragonite (Adapted with permission from [107]. Copyright 2017 American Chemical Society), and **f** granular aragonite recovered in fluidized-bed reactor (Adapted from [108] with permission from Elsevier)

demonstrated that the introduction of ethanol could enhance the stability of vaterite by forming calcium-ethanol complex. Up to 70% of the precipitated calcium carbonate retained as vaterite after being aged for 42 h.

The precipitation of calcium carbonate can be performed in fluidized-bed reactor (FBR) to suppress the homogeneous nucleation, generating calcium pellets with scarce water. The granular calcium carbonate is fluidized at a sufficient upflow rate, providing vast surface

Lin *et al. Sustainable Environment Research*   (2022) 32:45

Page 15 of 20

for crystallization. A precise control of supersaturation ratio is vital to ensure that the homogeneous nucleation is suppressed while the crystal growth and heterogeneous nucleation are favored [117]. The highest recovery of inorganic carbon as granule was at supersaturation ratio of 10.6. While most FBR adopt alien seed materials as fluidized medium, the purity of the resulting granules is compromised. Sioson et al. [118] proposed to synthesize calcium carbonate directly to produce homogeneous granules, i.e., no alien materials, as presented in Fig. 9f. The authors observed that the calcium-to-carbonate ratio dictated the size of granules and its settleability. The nucleation rate was described by pseudo-second order reaction rate, suggesting that the double-displacement chemical reaction of the precipitation of calcium carbonate.

The presence of impurity or additives can modify the surface of calcium carbonate, affecting the rate of dissolution and hence the polymorphs. Zhang et al. [119] studied the effect of the presence of Mg^{2+} on the formation of $CaCO_3$ crystals, particularly aragonite. It was demonstrated that at low Mg^{2+} concentration (Mg/Ca molar ratio of 0–1), amorphous calcium carbonate directly transforms into aragonite. The high Mg^{2+} concentrations (Mg/Ca molar ratio of 2–4) caused amorphous $CaCO_3$ to transform into monohydrocalcite first, followed by the gradual transformation into aragonite. The presence of ferrous ion influenced little on the formation of $CaCO_3$ at high supersaturation. However, the nucleation of $CaCO_3$ is inhibited by the ferrous ion at supersaturation ratio < 4 with respect of vaterite. Once the size of nucleus is greater than the critical value, the growth rate was promoted by iron ions [120]. The effect of using different absorbents during CO_2 capture has been studied. When ammonia was used as the absorbent, ammonium carbamate (NH_2COO^-) could be formed, which stabilized the metastable vaterite and resulted in a mixture of vaterite and calcite [121]. The existence of metastable polymorph is attributable to the slow desorption rate of the amine-absorbents, such as AMP [122]. In contrast, the use of MEA, diethanolamine and MDEA led to the formation of pure calcite crystal. This was because of the fast desorption rate of the amines, which enables the complete phase transformation to calcite [122].

5.2 Utilization of precipitated calcium carbonate

Calcium carbonate is widely used as fillers of paints, coatings, polymers, pigments, plastic and cement [123]. The precipitated calcium carbonate from the sequestration of CO_2 via indirect carbonation serves as potential substitutes to the present calcium carbonate that is synthesized from natural ores. The utilization of calcium carbonate derived from CO_2 sequestration

in cementless CaO-activated blast-furnace binder was studied [124]. The compressive strength of the specimen with 20 wt% precipitated calcium carbonate was 23% greater than the control specimen. The improvement in the mechanical strength is attributable to the filler effect and the reduction in pore size. The precipitated calcium carbonate from the carbonation of dolomite was used to as a filler of polyethersulfone hollow fiber membrane for oil-in-water filtration [125]. The introduction of 3 wt% aragonite improved the antifouling of the membrane by modifying the hydrophobicity of the membrane, enabling an oil reflection greater than 99% and water permeate flux of 102 L m^{-2} h^{-1}.

Life cycle analysis and techno-economic analysis have been performed to evaluate the potential of the utilization of precipitated calcium carbonate. Teir et al. [126] evaluated the economic and environmental feasibility of the production of calcium carbonate from stainless steel plating slags to replace the ground calcium carbonate used in papermaking. It was estimated that nearly 300 g of CO_2 can be avoided per kg of calcium carbonate produced. With the consideration of the revenue from calcium carbonate, investment and operation costs, a payback period of 2.2 years was projected. According the study of John et al. [127], the production of calcium carbonate by captured CO_2 using wollastonite resulted in an annual expenditure of 2.3 million US dollars. Therefore, the use of industrial waste as a feedstock of indirect carbonation is necessary to be profitable. Life cycle analysis has been conducted to evaluate the environmental benefit of utilizing the calcium carbonate that is produced by the carbonation of industrial waste with captured CO_2. Batuecas et al. [128] adopted the life-cycle analysis on the use of nano calcium carbonate produced from carbonation of waste produce as the filler of cement. Figure 10 depicts the optimized scenario to capture and utilize the CO_2 emitted during the clink production. While the conventional Portland cement exhibits a climate change category of 0.96 kg CO_{2eq} per kg of cement, the cement with 2 wt% of nano calcium carbonate obtained a value of 0.3 kg CO_{2eq} per kg of cement. Such result confirms that the utilization of the carbonized precipitate is capable of mitigating CO_2 emission more effectively. The scenario of the production of calcium carbonate from the indirect carbonation of steel converter slag was assessed by Mattila et al. [129]. The carbonation of steel converter slag features a negative CO_2 emission of 0.3 kg CO_{2eq} per kg of calcium carbonate, as compared to 1.04 kg CO_{2eq} per kg of calcium carbonate that is produced from natural limestone. Notably, the post-treatment such as recycling the washing water may contribute substantial carbon emission and environmental impact of the process.
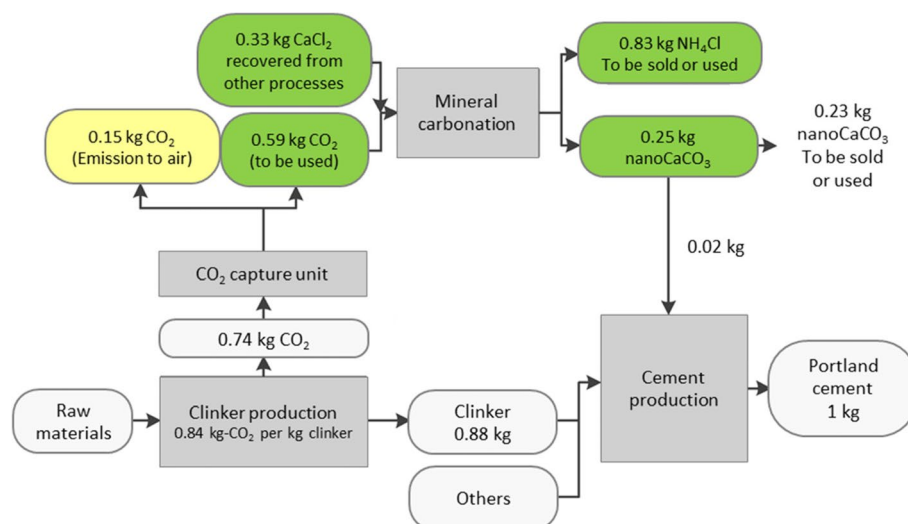
Fig. 10 Proposed production of cement with the utilization of calcium carbonate produced from the sequestration of CO_2 via indirect carbonation (Reproduced from [128] with permission from Elsevier)

6 Summary and future direction

Several advances have been made to incorporate chemical precipitation to enhance the effectiveness of carbon capture and sequestration. The precipitation and dissolution are dictated by the degree of supersaturation, which can be controlled by either temperature difference, pH swing, or the change of solution composition. In the capture of CO_2 from carbon-rich stream, the precipitation of CO_2-rich solid takes place, which can minimize the quantity of solvents to be regenerated and thus the heat duty. The precipitate that forms in chilled-ammonia process, is ammonium bicarbonate while those form in amine-based and amino acid-based solvents are carbamate and bicarbonates. In order to facilitate the precipitation of amino acid- and amine-based reagent, the solvent composition is crucial to tune its precipitability upon CO_2 absorption. The common solvents are alcohols, DMF and NMP. The future direction for the precipitation-incorporated carbon capture technology should be focused on the precise control of precipitation in order to prevent clogging and scaling in pipelines and reactor. The screening of effective phase-change solvent and amino acid/amine is also necessary to reduce the degradation of the reagent, the corrosion to the equipment and effective CO_2 absorption efficiency.

The mineral carbonation harnesses the dissolution of calcium and magnesium from silicates or industrial waste to precipitate CO_2 as thermodynamically stable carbonates, providing an effective way to sequester CO_2 without the need of leakage monitoring. The mineral carbonation can take place in situ with Mg- and Ca-rich silicates with

$scCO_2$. The water content and salinity of the $scCO_2$ were vital to enable a fast dissolution rate of silicates and prevent silica to form a passivating layer on surface. The phenomena are attributable to the hydration of the silicate surface and the inhibition of heterogeneous nucleation due to the high salinity. On the other hand, the ex-situ mineral carbonation can be optimized by the pretreatment of the feedstocks to enhance the dissolution of Ca^{2+} and Mg^{2+}. The activation includes the increase of surface area by comminution, the enhancement of leachability by thermal treatment, and the divide the dissolution and precipitation as two stages, i.e., indirect carbonation. The research direction of direct mineral carbonation lies in the inhibition of silica passivation and the enhancement of the reaction thickness of the feedstocks. The use of additives with surface selectivity may be used to regulate the dissolution and precipitation behavior. The indirect carbonation is recommended to focus on the maximation of the production of valuable products such as silica, carbonate minerals.

The precipitation of calcium carbonate is essential to optimize mineral carbonation. The morphology of calcium carbonate dictates its physicochemical properties which then define its usability. It is therefore crucial for technologies intended to produce this product to not only assess the purity, but the morphology as well. The generated product can also be subjected to tests to verify its usability. Most of the studies on the synthesis of $CaCO_3$ used chemicals as carbonate source instead of producing it from CO_2. For more advanced research, strategies on CO_2 capture using flue gas and feedstock materials must be incorporated in the assessment of the

Lin *et al. Sustainable Environment Research*   (2022) 32:45

Page 17 of 20

synthesis variables and methods. This will replicate more closely the actual process and give more accurate product characterization in order to gauge marketability.

Availability of data and materials
Not applicable.

Declarations

Competing interests
The authors declare they have no competing interests.

Author details
[1]Department of Civil and Environmental Engineering, University of Delaware, Newark, DE 19702, USA. [2]College of Engineering, National Graduate School of Engineering, University of the Philippines Diliman, Quezon City, Philippines. [3]Nanosystems Engineering Research Center for Nanotechnology-Enabled Water Treatment, Arizona State University, Tempe, AZ 85287-3005, USA. [4]Department of Environmental Engineering, National Chung Hsing University, Taichung 40227, Taiwan.

References

1. Ozkan M, Nayak SP, Ruiz AD, Jiang W. Current status and pillars of direct air capture technologies. iScience. 2022;25:103990.
2. USEIA. International Energy Outlook 2021. Washington, DC: US Energy Information Administration; 2021.
3. IPCC. Summary for Policymakers. In: Global Warming of 1.5 °C. An IPCC Special Report on the impacts of global warming of 1.5 °C above pre-industrial levels and related global greenhouse gas emission pathways, in the context of strengthening the global response to the threat of climate change, sustainable development, and efforts to eradicate poverty. Geneva: World Meteorological Organization; 2018. p. 32.
4. Boot-Handford ME, Abanades JC, Anthony EJ, Blunt MJ, Brandani S, Mac Dowell N, et al. Carbon capture and storage update. Energ Environ Sci. 2014;7:130–89.
5. Li B, Duan Y, Luebke D, Morreale B. Advances in CO_2 capture technology: A patent review. Appl Energ. 2013;102:1439–47.
6. McGurk SJ, Martín CF, Brandani S, Sweatman MB, Fan X. Microwave swing regeneration of aqueous monoethanolamine for post-combustion CO_2 capture. Appl Energ. 2017;192:126–33.
7. Zhang Z, Pan SY, Li H, Cai J, Olabi AG, Anthony EJ, et al. Recent advances in carbon dioxide utilization. Renew Sust Energ Rev. 2020;125:109799.
8. Wang T, Dong CD, Lin JY, Chen CW, Chang JS, Kim H, et al. Recent advances in carbon dioxide conversion: a circular bioeconomy perspective. Sustainability. 2021;13:6962.
9. Leung DYC, Caramanna G, Maroto-Valer MM. An overview of current status of carbon dioxide capture and storage technologies. Renew Sust Energ Rev. 2014;39:426–43.
10. Mayer B, Humez P, Becker V, Dalkhaa C, Rock L, Myrttinen A, et al. Assessing the usefulness of the isotopic composition of CO_2 for leakage monitoring at CO_2 storage sites: a review. Int J Greenh Gas Con. 2015;37:46–60.
11. Sanna A, Uibu M, Caramanna G, Kuusik R, M. Maroto-Valer M. A review of mineral carbonation technologies to sequester CO_2. Chem Soc Rev. 2014;43:8049–80.
12. Zhang S, Shen Y, Wang L, Chen J, Lu Y. Phase change solvents for post-combustion CO_2 capture: principle, advances, and challenges. Appl Energ. 2019;239:876–97.
13. N.Borhani T, Wang M. Role of solvents in CO_2 capture processes: the review of selection and design methods. Renew Sust Energ Rev. 2019;114:109299.
14. Gazzani M, Sutter D, Mazzotti M. Improving the efficiency of a chilled ammonia CO_2 capture plant through solid formation: a thermodynamic analysis. Energy Procedia. 2014;63:1084–90.
15. Snæbjörnsdóttir SÓ, Sigfússon B, Marieni C, Goldberg D, Gislason SR, Oelkers EH. Carbon dioxide storage through mineral carbonation. Nat Rev Earth Environ. 2020;1:90–102.
16. Liu W, Teng L, Rohani S, Qin Z, Zhao B, Xu CC, et al. CO_2 mineral carbonation using industrial solid wastes: A review of recent developments. Chem Eng J. 2021;416:129093.
17. Chang R, Kim S, Lee S, Choi S, Kim M, Park Y. Calcium carbonate precipitation for CO2 storage and utilization: a review of the carbonate crystallization and polymorphism. Front Energy Res. 2017;5:17.
18. Chao C, Deng Y, Dewil R, Baeyens J, Fan X. Post-combustion carbon capture. Renew Sust Energ Rev. 2021;138:110490.
19. Dirksen JA, Ring TA. Fundamentals of crystallization: Kinetic effects on particle size distributions and morphology. Chem Eng Sci. 1991;46:2389–427.
20. Karpinski PH, Wey JS. Precipitation processes. In: Myerson AS, editor. Handbook of industrial crystallization. 2nd ed. Woburn: Butterworth-Heinemann; 2002. p. 141–60.
21. Boch R. Carbonates in natural and geotechnical settings – chemical sediments as environmental archives. Jahrb Geol Bundesanst. 2020;159:67–130.
22. Galvão AC, Jiménez YP, Justel FJ, Robazza WS, Donatti FS. Salting-out precipitation of NaCl, KCl and NH_4Cl in mixtures of water and methanol described by the modified Pitzer model. J Chem Thermodyn. 2020;150:106202.
23. Han B, Sha Z, Partanen JI, Louhi-Kultanen M. Solubility of potassium dihydrogen phosphate in aqueous solutions of acetone, ethyl acetate, and thiourea from T = (298.15–313.15) K. Fluid Phase Equilibr. 2012;336:16–21.
24. Pokrovsky OS, Shirokova LS, Bénézeth P, Schott J, Golubev SV. Effect of organic ligands and heterotrophic bacteria on wollastonite dissolution kinetics. Am J Sci. 2009;309:731–72.
25. Schott J, Pokrovsky OS, Spalla O, Devreux F, Gloter A, Mielczarski JA. Formation, growth and transformation of leached layers during silicate minerals dissolution: the example of wollastonite. Geochim Cosmochim Ac. 2012;98:259–81.
26. Sear RP. Nucleation: theory and applications to protein solutions and colloidal suspensions. J Phys-Condens Matter. 2007;19:033101.
27. Nielsen AE. Electrolyte crystal growth mechanisms. J Cryst Growth. 1984;67:289–310.
28. Crundwell FK. The mechanism of dissolution of forsterite, olivine and minerals of the orthosilicate group. Hydrometallurgy. 2014;150:68–82.
29. Reza J, Trejo A. Degradation of aqueous solutions of alkanolamine blends at high temperature, under the presence of CO_2 and H_2S. Chem Eng Commun. 2006;193:129–38.
30. Guo H, Li C, Shi X, Li H, Shen S. Nonaqueous amine-based absorbents for energy efficient CO_2 capture. Appl Energ. 2019;239:725–34.
31. Li X, Liu J, Jiang W, Gao G, Wu F, Luo C, et al. Low energy-consuming CO_2 capture by phase change absorbents of amine/alcohol/H_2O. Sep Purif Technol. 2021;275:119181.
32. Li Y, Cheng J, Hu L, Liu N, Zhou J, Cen K. Regulating crystal structures of EDA-carbamates in solid–liquid phase-changing CO_2 capture solutions. Fuel. 2019;252:47–54.
33. Gao X, Li X, Cheng S, Lv B, Jing G, Zhou Z. A novel solid–liquid 'phase controllable' biphasic amine absorbent for CO_2 capture. Chem Eng J. 2022;430:132932.
34. Liu F, Jing G, Zhou X, Lv B, Zhou Z. Performance and mechanisms of triethylene tetramine (TETA) and 2-amino-2-methyl-1-propanol

Lin *et al. Sustainable Environment Research*   (2022) 32:45

Page 18 of 20

(AMP) in aqueous and nonaqueous solutions for CO_2 capture. ACS Sustain Chem Eng. 2018;6:1352–61.

35. Gal E. Ultra cleaning of combustion gas including the removal of CO_2. Patent WO2006022885. Geneva: World Intellectual Property Organization; 2006.

36. Sutter D, Gazzani M, Mazzotti M. A low-energy chilled ammonia process exploiting controlled solid formation for post-combustion CO_2 capture. Faraday Discuss. 2016;192:59–83.

37. Milella F, Mazzotti M. Estimation of the growth and the dissolution kinetics of ammonium bicarbonate in aqueous ammonia solutions from batch crystallization experiments. Cryst Growth Des. 2019;19:5907–22.

38. Sanchez-Fernandez E, Mercader F de M, Misiak K, van der Ham L, Linders M, Goetheer E. New process concepts for CO_2 capture based on precipitating amino acids. Energy Procedia. 2013;37:1160–71.

39. Eide-Haugmo I, Brakstad OG, Hoff KA, da Silva EF, Svendsen HF. Marine biodegradability and ecotoxicity of solvents for CO_2-capture of natural gas. Int J Greenh Gas Con. 2012;9:184–92.

40. Holst J van, Versteeg GF, Brilman DWF, Hogendoorn JA. Kinetic study of CO_2 with various amino acid salts in aqueous solution. Chem Eng Sci. 2009;64:59–68.

41. Ramezani R, Mazinani S, Felice RD. State-of-the-art of CO_2 capture with amino acid salt solutions. Rev Chem Eng. 2022;38:273–99.

42. Ciftja AF, Hartono A, Svendsen HF. Selection of amine amino acids salt systems for CO_2 capture. Energy Procedia. 2013;37:1597–604.

43. Sanchez Fernandez E, Heffernan K, van der Ham LV, Linders MJG, Eggink E, Schrama FNH, et al. Conceptual design of a novel CO_2 capture process based on precipitating amino acid solvents. Ind Eng Chem Res. 2013;52:12223–35.

44. Alivand MS, Mazaheri O, Wu Y, Stevens GW, Scholes CA, Mumford KA. Development of aqueous-based phase change amino acid solvents for energy-efficient CO_2 capture: the role of antisolvent. Appl Energ. 2019;256:113911.

45. Chen S, Wu Y, Stevens GW, Hu G, Sun W, Mumford KA. Precipitation study of CO_2-loaded glycinate solution with the introduction of ethanol as an antisolvent. Front Chem Sci Eng. 2020;14:415–24.

46. Nduagu E. Production of Mg(OH)2 from Mg-silicate rock for CO_2 mineral sequestration. Doctoral dissertation [Ph.D. Dissertation]. Turku: Åbo Akademi Univ; 2012.

47. Markewitz P, Kuckshinrichs W, Leitner W, Linssen J, Zapp P, Bongartz R, et al. Worldwide innovations in the development of carbon capture technologies and the utilization of CO_2. Energ Environ Sci. 2012;5:7281–305.

48. Romanov V, Soong Y, Carney C, Rush GE, Nielsen B, O'Connor W. Mineralization of carbon dioxide: a literature review. ChemBioEng Rev. 2015;2:231–56.

49. Cuellar-Franca R, Azapagic A. Carbon capture, storage and utilisation technologies: a critical analysis and comparison of their life cycle environmental impacts. J CO_2 Util. 2015;9:82–102.

50. Olajire AA. A review of mineral carbonation technology in sequestration of CO_2. J Petrol Sci Eng. 2013;109:364–92.

51. Kharaka YK, Thordsen JJ, Hovorka SD, Seay Nance H, Cole DR, Phelps TJ, et al. Potential environmental issues of CO_2 storage in deep saline aquifers: geochemical results from the Frio-I Brine Pilot test, Texas, USA. Appl Geochem. 2009;24:1106–12.

52. Kwak JH, Hu JZ, Turcu RVF, Rosso KM, Ilton ES, Wang C, et al. The role of H_2O in the carbonation of forsterite in supercritical CO_2. Int J Greenh Gas Con. 2011;5:1081–92.

53. Placencia-Gómez E, Kerisit SN, Mehta HS, Qafoku O, Thompson CJ, Graham TR, et al. Critical water coverage during forsterite carbonation in thin water films: activating dissolution and mass transport. Environ Sci Technol. 2020;54:6888–99.

54. Loring JS, Thompson CJ, Wang Z, Joly AG, Sklarew DS, Schaef HT, et al. In situ infrared spectroscopic study of forsterite carbonation in wet supercritical CO_2. Environ Sci Technol. 2011;45:6204–10.

55. Pasquier L-C, Mercier G, Blais J-F, Cecchi E, Kentish S. Reaction mechanism for the aqueous-phase mineral carbonation of heat-activated serpentine at low temperatures and pressures in flue gas conditions. Environ Sci Technol. 2014;48:5163–70.

56. Min Y, Li Q, Voltolini M, Kneafsey T, Jun YS. Wollastonite carbonation in water-bearing supercritical CO_2: effects of particle size. Environ Sci Technol. 2017;51:13044–53.

57. Wang F, Giammar DE. Forsterite dissolution in saline water at elevated temperature and high CO_2 pressure. Environ Sci Technol. 2013;47:168–73.

58. Wang F, Dreisinger D, Jarvis M, Hitchins T. Kinetics and mechanism of mineral carbonation of olivine for CO_2 sequestration. Miner Eng. 2019;131:185–97.

59. Huijgen WJJ, Witkamp G-J, Comans RNJ. Mechanisms of aqueous wollastonite carbonation as a possible CO_2 sequestration process. Chem Eng Sci. 2006;61:4242–51.

60. Felmy AR, Qafoku O, Arey BW, Hu JZ, Hu M, Todd Schaef H, et al. Reaction of water-saturated supercritical CO_2 with forsterite: evidence for magnesite formation at low temperatures. Geochim Cosmochim Ac. 2012;91:271–82.

61. Dlugogorski BZ, Balucan RD. Dehydroxylation of serpentine minerals: implications for mineral carbonation. Renew Sust Energ Rev. 2014;31:353–67.

62. Du Breuil C, Pasquier LC, Dipple G, Blais J-F, Iliuta MC, Mercier G. Impact of particle size in serpentine thermal treatment: implications for serpentine dissolution in aqueous-phase using CO_2 in flue gas conditions. Appl Clay Sci. 2019;182:105286.

63. Johnson NC, Thomas B, Maher K, Rosenbauer RJ, Bird D, Brown GE. Olivine dissolution and carbonation under conditions relevant for in situ carbon storage. Chem Geol. 2014;373:93–105.

64. Kashim MZ, Tsegab H, Rahmani O, Abu Bakar ZA, Aminpour SM. Reaction mechanism of wollastonite in situ mineral carbonation for CO_2 sequestration: effects of saline conditions, temperature, and pressure. ACS Omega. 2020;5:28942–54.

65. Wang F, Dreisinger D, Jarvis M, Hitchins T, Dyson D. Quantifying kinetics of mineralization of carbon dioxide by olivine under moderate conditions. Chem Eng J. 2019;360:452–63.

66. Orlando A, Borrini D, Marini L. Dissolution and carbonation of a serpentinite: Inferences from acid attack and high P–T experiments performed in aqueous solutions at variable salinity. Appl Geochem. 2011;26:1569–83.

67. Turri L, Gérardin K, Muhr H, Lapicque F, Saravia A, Szenknect S, et al. CO_2 sequestration by carbonation of olivine: a new process for optimal separation of the solids produced. Green Process Synth. 2019;8:480–7.

68. Gérardin K, Turri L, Muhr H, Gérard A, Lagadic A, Bertucci A, et al. Towards viable CO_2 sequestration: Production of high specific surface area silica by olivine dissolution in concentrated acidic solutions. J Clean Prod. 2019;211:1547–52.

69. Raza W, Raza N, Agbe H, Kumar RV, Kim KH, Yang J. Multistep sequestration and storage of CO_2 to form valuable products using forsterite. Energy. 2018;155:865–73.

70. Baena-Moreno FM, Rodríguez-Galán M, Vega F, Alonso-Fariñas B, Vilches Arenas LF, Navarrete B. Carbon capture and utilization technologies: a literature review and recent advances. Energy Source Part A. 2019;41:1403–33.

71. Bobicki ER, Liu Q, Xu Z, Zeng H. Carbon capture and storage using alkaline industrial wastes. Prog Energy Combust. 2012;38:302–20.

72. Ahmaruzzaman M. A review on the utilization of fly ash. Prog Energy Combust. 2010;36:327–63.

73. Özbay E, Erdemir M, Durmuş Hİ. Utilization and efficiency of ground granulated blast furnace slag on concrete properties – a review. Constr Build Mater. 2016;105:423–34.

74. Song Q, Guo M-Z, Wang L, Ling T-C. Use of steel slag as sustainable construction materials: a review of accelerated carbonation treatment. Resour Conserv Recy. 2021;173:105740.

75. Rai S, Wasewar K, Agnihotri A. Treatment of alumina refinery waste (red mud) through neutralization techniques: a review. Waste Manage Res. 2017;35:563–80.

76. Wang B, Pan Z, Cheng H, Zhang Z, Cheng F. A review of carbon dioxide sequestration by mineral carbonation of industrial byproduct gypsum. J Clean Prod. 2021;302:126930.

77. Ukwattage NL, Ranjith PG, Yellishetty M, Bui HH, Xu T. A laboratory-scale study of the aqueous mineral carbonation of coal fly ash for CO_2 sequestration. J Clean Prod. 2015;103:665–74.

78. Hosseini T, Haque N, Selomulya C, Zhang L. Mineral carbonation of Victorian brown coal fly ash using regenerative ammonium chloride

Lin *et al. Sustainable Environment Research*   (2022) 32:45

Page 19 of 20

– process simulation and techno-economic analysis. Appl Energ. 2016;175:54–68.

79. Eloneva S, Teir S, Salminen J, Fogelholm CJ, Zevenhoven R. Fixation of CO_2 by carbonating calcium derived from blast furnace slag. Energy. 2008;33:1461–7.

80. Ukwattage NL, Ranjith PG, Li X. Steel-making slag for mineral sequestration of carbon dioxide by accelerated carbonation. Measurement. 2017;97:15–22.

81. Yadav S, Mehra A. Experimental study of dissolution of minerals and CO_2 sequestration in steel slag. Waste Manage. 2017;64:348–57.

82. Chen TL, Jiang W, Shen AL, Chen YH, Pan SY, Chiang PC. CO_2 mineralization and utilization using various calcium-containing wastewater and refining slag via a high-gravity carbonation process. Ind Eng Chem Res. 2020;59:7140–50.

83. Chu DH, Vinoba M, Bhagiyalakshmi M, Baek IH, Nam SC, Yoon Y, et al. CO_2 mineralization into different polymorphs of $CaCO_3$ using an aqueous-CO_2 system. RSC Adv. 2013;3:21722–9.

84. Song K, Kim W, Park S, Bang JH, Jeon CW, Ahn JW. Effect of polyacrylic acid on direct aqueous mineral carbonation of flue gas desulfurization gypsum. Chem Eng J. 2016;301:51–7.

85. Tan W, Zhang Z, Li H, Li Y, Shen Z. Carbonation of gypsum from wet flue gas desulfurization process: experiments and modeling. Environ Sci Pollut R. 2017;24:8602–8.

86. Song K, Jang Y-N, Kim W, Lee MG, Shin D, Bang J-H, et al. Factors affecting the precipitation of pure calcium carbonate during the direct aqueous carbonation of flue gas desulfurization gypsum. Energy. 2014;65:527–32.

87. Du Y, Fu C, Gong B, Miao E, Zheng X, Xiong Z, et al. Real-time investigation of the CO_2 mineral carbonation reaction rate through direct aqueous route using semi-dry desulfurization slag. J CO_2 Util. 2021;51:101614.

88. Yan Z, Wang Y, Yue H, Liu C, Zhong S, Ma K, et al. Integrated process of monoethanolamine-based CO_2 absorption and CO_2 mineralization with SFGD slag: process simulation and life-cycle assessment of CO_2 emission. ACS Sustain Chem Eng. 2021;9:8238–48.

89. Ragipani R, Escobar E, Prentice D, Bustillos S, Simonetti D, Sant G, et al. Selective sulfur removal from semi-dry flue gas desulfurization coal fly ash for concrete and carbon dioxide capture applications. Waste Manage. 2021;121:117–26.

90. Lin JY, Kim M, Li D, Kim H, Huang C. The removal of phosphate by thermally treated red mud from water: the effect of surface chemistry on phosphate immobilization. Chemosphere. 2020;247:125867.

91. Liang G, Chen W, Nguyen AV, Nguyen TAH. Red mud carbonation using carbon dioxide: Effects of carbonate and calcium ions on goethite surface properties and settling. J Colloid Interf Sci. 2018;517:230–8.

92. Yadav VS, Prasad M, Khan J, Amritphale SS, Singh M, Raju CB. Sequestration of carbon dioxide (CO_2) using red mud. J Hazard Mater. 2010;176:1044–50.

93. Kashefi K, Pardakhti A, Shafiepour M, Hemmati A. Process optimization for integrated mineralization of carbon dioxide and metal recovery of red mud. J Environ Chem Eng. 2020;8:103638.

94. Kusin FM, Hasan SNMS, Hassim MA, Molahid VLM. Mineral carbonation of sedimentary mine waste for carbon sequestration and potential reutilization as cementitious material. Environ Sci Pollut R. 2020;27:12767–80.

95. Mohd Isha NS, Mohd Kusin F, Ahmad Kamal NM, Hasan SNMS, Molahid VLM. Geochemical and mineralogical assessment of sedimentary limestone mine waste and potential for mineral carbonation. Environ Geochem Hlth. 2021;43:2065–80.

96. Molahid VLM, Kusin FM, Kamal NMA, Hasan SNMS, Ramli NAA, Abdullah AM, et al. Carbon sequestration of limestone mine waste through mineral carbonation and utilization as supplementary cementitious material. Int J Integr Eng. 2021;13:311–20.

97. Khalidy R, Santos RM. The fate of atmospheric carbon sequestrated through weathering in mine tailings. Miner Eng. 2021;163:106767.

98. Oskierski HC, Dlugogorski BZ, Jacobsen G. Sequestration of atmospheric CO_2 in chrysotile mine tailings of the Woodsreef Asbestos Mine, Australia: quantitative mineralogy, isotopic fingerprinting and carbonation rates. Chem Geol. 2013;358:156–69.

99. Power IM, Dipple GM, Bradshaw PMD, Harrison AL. Prospects for CO_2 mineralization and enhanced weathering of ultramafic mine tailings

from the Baptiste nickel deposit in British Columbia, Canada. Int J Greenh Gas Con. 2020;94.

100. Goodwin AL, Michel FM, Phillips BL, Keen DA, Dove MT, Reeder RJ. Nanoporous structure and medium-range order in synthetic amorphous calcium carbonate. Chem Mater. 2010;22:3197–205.

101. Jimoh OA, Ariffin KS, Hussin H Bin, Temitope AE. Synthesis of precipitated calcium carbonate: a review. Carbonate Evaporite. 2018;33:331–46.

102. Declet A, Reyes E, Suárez OM. Calcium carbonate precipitation: a review of the carbonate crystallization process and applications in bioinspired composites. Rev Adv Mater Sci. 2016;44:87–107.

103. Tan WL, Ahmad AL, Leo CP, Lam SS. A critical review to bridge the gaps between carbon capture, storage and use of $CaCO_3$. J CO_2 Util. 2020;42:101333.

104. Rodriguez-Blanco JD, Shaw S, Benning LG. The kinetics and mechanisms of amorphous calcium carbonate (ACC) crystallization to calcite, viavaterite. Nanoscale. 2011;3:265–71.

105. Zhao H, Park Y, Lee DH, Park AHA. Tuning the dissolution kinetics of wollastonite via chelating agents for CO_2 sequestration with integrated synthesis of precipitated calcium carbonates. Phys Chem Chem Phys. 2013;15:15185–92.

106. Liendo F, Arduino M, Deorsola FA, Bensaid S. Optimization of $CaCO_3$ synthesis through the carbonation route in a packed bed reactor. Powder Technol. 2021;377:868–81.

107. Chang R, Choi D, Kim MH, Park Y. Tuning crystal polymorphisms and structural investigation of precipitated calcium carbonates for CO_2 mineralization. ACS Sustain Chem Eng. 2017;5:1659–67.

108. de Luna MDG, Sioson AS, Choi AES, Abarca RRM, Huang YH, Lu MC. Operating pH influences homogeneous calcium carbonate granulation in the frame of CO_2 capture. J Clean Prod. 2020;272:122325.

109. Shen Q, Wei H, Wang L, Zhou Y, Zhao Y, Zhang Z, et al. Crystallization and aggregation behaviors of calcium carbonate in the presence of poly(vinylpyrrolidone) and sodium dodecyl sulfate. J Phys Chem B. 2005;109:18342–7.

110. Abebe M, Hedin N, Bacsik Z. Spherical and porous particles of calcium carbonate synthesized with food friendly polymer additives. Cryst Growth Des. 2015;15:3609–16.

111. Tai CY, Chen FB. Polymorphism of $CaCO_3$ precipitated in a constant-composition environment. AIChE J. 1998;44:1790–8.

112. Ramakrishna C, Thenepalli T, Huh JH, Ahn JW. Precipitated calcium carbonate synthesis by simultaneous injection to produce nano whisker aragonite. J Korean Ceram Soc. 2016;53:222–6.

113. Luo X, Song X, Cao Y, Song L, Bu X. Investigation of calcium carbonate synthesized by steamed ammonia liquid waste without use of additives. RSC Adv. 2020;10:7976–86.

114. Cui ZG, Cui CF, Zhu Y, Binks BP. Multiple phase inversion of emulsions stabilized by in situ surface activation of $CaCO_3$ nanoparticles via adsorption of fatty acids. Langmuir. 2012;28:314–20.

115. Nakamura J, Poologasundarampillai G, Jones JR, Kasuga T. Tracking the formation of vaterite particles containing aminopropyl-functionalized silsesquioxane and their structure for bone regenerative medicine. J Mater Chem B. 2013;1:4446–54.

116. Jiang J, Wu Y, Chen C, Wang X, Zhao H, Xu S, et al. A novel route to prepare the metastable vaterite phase of $CaCO_3$ from $CaCl_2$ ethanol solution and Na2CO3 aqueous solution. Adv Powder Technol. 2018;29:2416–22.

117. Huang YH, Garcia-Segura S, de Luna MDG, Sioson AS, Lu MC. Beyond carbon capture towards resource recovery and utilization: fluidized-bed homogeneous granulation of calcium carbonate from captured CO_2. Chemosphere. 2020;250:126325.

118. Sioson AS, Choi AES, de Luna MDG, Huang YH, Lu MC. Calcium carbonate granulation in a fluidized-bed reactor: kinetic, parametric and granule characterization analyses. Chem Eng J. 2020;382:122879.

119. Zhang Z, Xie Y, Xu X, Pan H, Tang R. Transformation of amorphous calcium carbonate into aragonite. J Cryst Growth. 2012;343:62–7.

120. Korchef A. Effect of iron ions on the crystal growth kinetics and microstructure of calcium carbonate. Cryst Growth Des. 2019;19:6893–902.

121. Konopacka-Łyskawa D, Kościelska B, Karczewski J, Gołąbiewska A. The influence of ammonia and selected amines on the characteristics of calcium carbonate precipitated from calcium chloride solutions via carbonation. Mater Chem Phys. 2017;193:13–8.

Lin *et al. Sustainable Environment Research*　　(2022) 32:45

Page 20 of 20

122. Arti M, Youn MH, Park KT, Kim HJ, Kim YE, Jeong SK. Single process for CO_2 capture and mineralization in various alkanolamines using calcium chloride. Energ Fuel. 2017;31:763–9.

123. Boyjoo Y, K. Pareek V, Liu J. Synthesis of micro and nano-sized calcium carbonate particles and their applications. J Mater Chem A. 2014;2:14270–88.

124. Jeong Y, Yum WS, Moon J, Oh JE. Utilization of precipitated $CaCO_3$ from carbon sequestration of industrially emitted CO_2 in cement-less CaO-activated blast-furnace slag binder system. J Clean Prod. 2017;166:649–59.

125. Jimoh OA, Okoye PU, Otitoju TA, Ariffin KS. Aragonite precipitated calcium carbonate from magnesium rich carbonate rock for polyethersulfone hollow fibre membrane application. J Clean Prod. 2018;195:79–92.

126. Teir S, Kotiranta T, Pakarinen J, Mattila HP. Case study for production of calcium carbonate from carbon dioxide in flue gases and steelmaking slag. J CO_2 Util. 2016;14:37–46.

127. John JM, Wan Alwi SR, Omoregbe DI. Techno-economic analysis of carbon dioxide capture and utilisation analysis for an industrial site with fuel cell integration. J Clean Prod. 2021;281:124920.

128. Batuecas E, Liendo F, Tommasi T, Bensaid S, Deorsola FA, Fino D. Recycling CO_2 from flue gas for $CaCO_3$ nanoparticles production as cement filler: a life cycle assessment. J CO_2 Util. 2021;45:101446.

129. Mattila HP, Hudd H, Zevenhoven R. Cradle-to-gate life cycle assessment of precipitated calcium carbonate production from steel converter slag. J Clean Prod. 2014;84:611–8.

Publisher's Note